

ReLaX-Net: Reusing Layers for Parameter-Efficient Physical Neural Networks

Kohei Tsuchiyama¹, André Röhm^{1*}, Takatomo Mihana¹,
Ryoichi Horisaki¹

¹Graduate School of Information Science and Technology, The
University of Tokyo, 7-3-1 Hongo, Bunkyo-ku, 113-8656, Tokyo, Japan.

*Corresponding author(s). E-mail(s): roehm@g.ecc.u-tokyo.ac.jp;
Contributing authors: tsuchiyama-kohei655@g.ecc.u-tokyo.ac.jp;
takatomo_mihana@ipc.i.u-tokyo.ac.jp; horisaki@g.ecc.u-tokyo.ac.jp;

Abstract

Physical Neural Networks (PNN) are promising platforms for next-generation computing systems. However, recent advances in digital neural network performance are largely driven by the rapid growth in the number of trainable parameters and, so far, demonstrated PNNs are lagging behind by several orders of magnitude in terms of scale. This mirrors size and performance constraints found in early digital neural networks. In that period, efficient reuse of parameters contributed to the development of parameter-efficient architectures such as convolutional neural networks.

In this work, we numerically investigate hardware-friendly weight-tying for PNNs. Crucially, with many PNN systems, there is a time-scale separation between the fast dynamic active elements of the forward pass and the only slowly trainable elements implementing weights and biases. With this in mind, we propose the Reuse of Layers for eXpanding a Neural Network (ReLaX-Net) architecture, which employs a simple layer-by-layer time-multiplexing scheme to increase the effective network depth and efficiently use the number of parameters. We only require the addition of fast switches for existing PNNs. We validate ReLaX-Nets via numerical experiments on image classification and natural language processing tasks. Our results show that ReLaX-Net improves computational performance with only minor modifications to a conventional PNN. We observe a favorable scaling, where ReLaX-Nets exceed the performance of equivalent traditional RNNs or DNNs with the same number of parameters.

Keywords: Physical Computing, Neuromorphic Computing, Recurrent Neural Network

Keywords: Physical Computing, Neuromorphic Computing, Recurrent Neural Network

1 Introduction

Artificial Intelligence (AI) technologies have made remarkable strides in areas such as image recognition [1, 2, 3, 4] and natural language processing [5, 6]. As the potential economic usages appear closer, the demand for computational power for AI is surging accordingly. Until now, this demand has to be met by newer and more powerful data centers, based on semiconductor technologies. However, these technologies are expected to increasingly face fundamental physical limitations in the near future. One of the major concerns is the surge in power consumption as clock frequencies reach beyond gigahertz levels, resulting in excessive heat generation. Furthermore, quantum effects begin to interfere with electron behavior at cutting-edge semiconductor scales, resulting in increased transistor errors and reduced calculation reliability. Consequently, there is a pressing need to develop new information processing units that offer high-speed, energy-efficient computing. In response, researchers are actively exploring alternative avenues, from novel materials and architectures to the investigation of new computational paradigms.

A Physical Neural Network (PNN) describes the concept of implementing a neural network with technologies on other physical substrates such as optics [7, 8, 9, 10, 11, 12, 13, 14, 15, 16], spintronics [17, 18, 19], and chemitronics [20, 21]. PNNs are often, but not necessarily, analog, and they may employ setups which do not separate memory and computation, thus differing from traditional von Neumann architectures. PNNs ultimately aim to surpass conventional silicon-transistor systems by utilizing new physical characteristics for computing and to become the next generation of computing systems for implementing artificial neural networks.

Recent advances in AI performance are largely driven by the rapid growth in the number of trainable parameters of neural network models. Thus, PNNs must also support a comparable number of parameters to be competitive with current systems. For example, in Large Language Models (LLM), it is well known that increasing the number of parameters improves performance, as long as sufficient training time and data [34] also exists. Therefore, to produce ever better LLMs, significant effort has been devoted to scaling up the size [35]. However, the number of parameters in published and demonstrated PNNs is low and, arguably, stagnating compared to that in conventional machine learning models (see Fig. 1). While recent LLMs have sizes of hundreds of billions of trainable parameters [27] (Fig. 1, blue dots), the largest PNN demonstrations do not even reach a million (Fig. 1, other colors). For one, physical constraints inherent to non-electronic devices pose significant challenges to scaling up layer-wise parameters in neural networks. For example, diffraction divergence and physical footprint limit integration density in free space optics [36], thermal crosstalk and footprint-loss tradeoff restrict scaling in integrated photonic circuits [37, 38], and coupling overhead and device variability hinder enlarging in spintronics [39]. These challenges often require large and complex architectures to overcome, resulting in

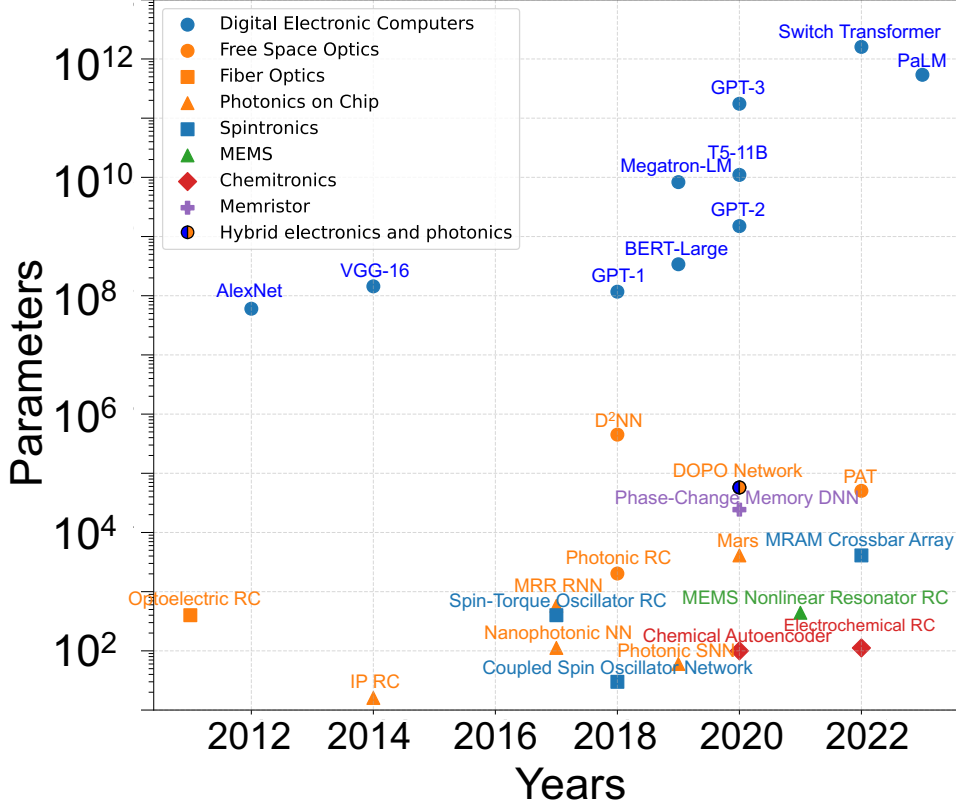


Fig. 1 Parameter growth of machine learning models on Electronic Computers and Physical Neural Networks. On conventional computers, the model sizes (AlexNet [22], VGG16 [2], GPT-1 [23], BERT-Large [6], Megatron-LM [24], GPT-2 [25], T5-11B [26], GPT-3 [27], Switch Transformer [28], PaLM [29]) grow rapidly. On the other hand, the PNN models (Optoelectric Reservoir Computing (RC) [8], Photonic Integrated (PI) RC [9], Nanophotonic Neural Network (NN) [10], Spin-Torque Oscillator RC [17], Micro-Ring Resonator (MRR) Recurrent Neural Network (RNN) [11], Coupled Spin Oscillator Network [19], Photonic SNN (Spiking Neurosynaptic Network) [30], Photonic RC [12], Memristor [31], Diffractive Deep Neural Network (D²NN) [13], Chemical Autoencoder [20], Mars [14], MEMS [32], Electrochemical RC [21], Magnetoresistive Random-Access Memory (MRAM) Crossbar Array [15], Physical Aware Training (PAT) [16] and Degenerate Optical Parametric Oscillator (DOPO) Network [33]) also grow gradually, but there is a huge gap between Electronic Computers and Physical Neural Networks. See Supplemental Information Section S1 for details.

cost problems [40]. As a result, no existing PNN has yet matched the computational capacity of high-end electronic systems.

As the raw number of parameters of PNNs is likely to remain below those of electronic systems, we must investigate alternative forms of using the existing sizes effectively. These constraints mirror the size restrictions found in early digital neural networks and one can take inspiration from relevant papers of the era. For example, the development of Convolutional Neural Networks (CNNs) was, in part, driven by a

need to be parameter-efficient [41]. Similarly, auto-encoders commonly were developed for both preserving the symmetry of the encoding operation and reduction in computational demands [42]. Here, the common insight was the following: Even when the number of trainable weights is fixed, one can still increase the size of the neural network — if one allows the re-use of components. In CNNs, this takes the form of convolutional kernels, which are applied over many areas of the image. A convolutional layer is equivalent to a regular fully-connected layer whose weight matrix is constrained by the convolutional kernel [41]. “Weight-sharing” or “tying weights” is useful for engineering neural networks towards specific tasks, and the study of weight-sharing is an ongoing topic of research, in particular on general models of weight-tying [43].

Weight-sharing in PNNs remains underexplored. Here, weight-sharing would only help alleviate hardware costs and complexity if the same weights were implemented only once, without duplication. This necessitates the re-use of hardware for multiple purposes. Time-multiplexing is the most promising mechanism. It allows the re-use of entire structures, by temporally staggering the information processing. We are therefore motivated to explore unique ways in which PNNs can scale using weight-sharing and time-multiplexing, which may not have necessarily been considered for digital silicon-transistor based ANNs.

In this paper, we introduce the Reuse of Layers for eXpanding a Neural Network (ReLaX-Net) architecture to increase the capability of PNNs. ReLaX-Net uses a small set of layers and switches between them at each calculation time step. A simple periodic switching strategy strikes a balance between parameter scalability and implementation complexity. When integrated into an existing photonic RNN, ReLaX-Net requires only the addition of switching elements. In general, there is no need to replicate nonlinear activation components or reconfigure the entire network at high rates. Furthermore, ReLaX-Net can be interpreted as a model representing an Intermediate-scale PNN, which is positioned between conventional small PNNs with static weights and the fully dynamic large PNNs of the future. Just as “Noisy Intermediate-Scale Quantum computing” (NISQ) [44] is seen as an intermediate step towards general use in quantum computing, the ReLaX-Net architecture is mainly motivated with the limitations of near-future PNNs in mind.

The remainder of this paper is structured as follows. We provide an overview of the idea of time-multiplexing, and how it can connect concepts from recurrent neural networks and feed-forward neural networks in Sec. 2. We showcase how time-multiplexing allows the reuse of hardware, and how it can lead to weight-shared architectures. We put particular emphasis on how time-multiplexing can differ between PNNs and digital networks. We then introduce the ReLaX-Net framework and explain its advantages in Sec. 3. We demonstrate how reusing layers improves performance in a parameter-efficient way on image classification and natural language processing tasks in Sec. 4. Finally, we summarize this study and clarify current limitations and perspectives.

2 Time-multiplexing of Neural Networks

Consider a standard multi-layer perceptron with N neurons forming the hidden states $h_l \in \mathbb{R}^N$ for the layers $l \in \{0, \dots, L\}$ where $l = 0$ corresponds to the input state.

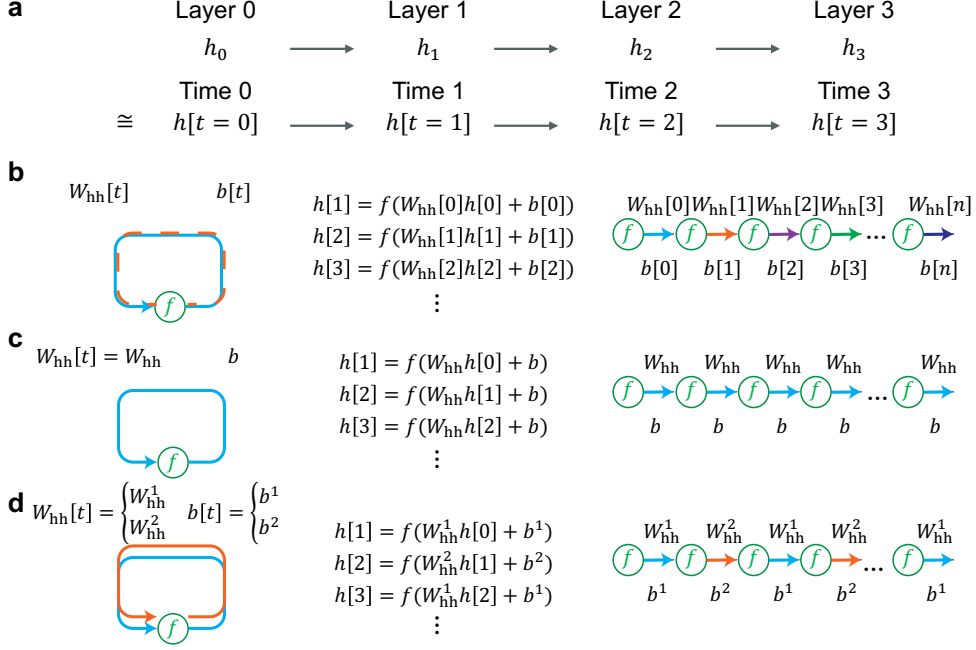


Fig. 2 Concepts of “time multiplexing”. **a**: While the state h_l in a conventional network evolves when passing through distinct layers l , in a time-multiplexed system the state $h[t]$ evolves over several time steps t (see Eq. (3)). **b**: By reusing the same nonlinear element, but reconfiguring the weights network weights $W_{hh}[t]$ (and biases $b[t]$) at each step t , we can reproduce the dynamics of a standard DNN (Eq. (3)). **c**: If the matrix W_{hh} (and bias) is fixed (independent of t), the system implements a standard RNN (Eq. (5)). **d**: The network weight W_{hh} and biases $b[t]$ are switched periodically at every time step for the ReLaX-net architecture proposed in Sec. 3.

The core mathematical operation of the forward pass using the nonlinear activation function f is typically formulated as

$$h_{l+1} = f(W_{hh}^l h_l + b_l), \quad (1)$$

$$\hat{y} = W_{hy} h_L + b_y \quad (2)$$

where the entries of the hidden-hidden weight matrices $W_{hh} \in \mathbb{R}^{N \times N}$, the hidden-output weight matrices $W_{hy}^l \in \mathbb{R}^{N \times Y}$ and bias terms $b_l \in \mathbb{R}^N$, $b_y \in \mathbb{R}^Y$ are to be determined via training. We consider a constant hidden state dimension N for all l here for simplicity, but the argument can in principle be generalized. Physical Neural Networks (PNNs) must consider how to emulate this functionality in hardware. The most straightforward way is to create a separate physical neuron for each dimension of h and for each layer l , each implementing the nonlinear activation function f . These physical neurons then must be connected with adjustable weights to emulate the effects of the weight matrix W_{hh}^l for every layer l . Thus, $N \times L$ dynamically changing variables are needed for simulating the evolution of the states h_l , as well as $N^2 L + N L$ trainable

parameters for implementing the weights and biases. But typically, having such a one-to-one correspondence of physical components and layers is hardware-inefficient.

The idea of “time multiplexing” can drastically reduce the hardware need — by trading spatial complexity for temporal complexity. Via time-multiplexing, we can replace the notion of distinct layers with distinct points in time. We follow the time-evolution of the hidden state $h[t] \in \mathbb{R}^N$ for $t \in [0, \dots, L_T]$ via

$$h[t + 1] = f(W_{\text{hh}}[t] h[t] + b[t]). \quad (3)$$

$$\hat{y} = W_{\text{hy}} h[L_T] + b_y \quad (4)$$

As sketched by Fig. 2a, using this simple correspondence between time and layers, we can reduce the number of physical elements. Now, instead of information of distinct layers of the neural network being physically located in separate elements, we reuse the hidden state $h[t]$, the weights $W_{\text{hh}}[t]$ and bias terms $b[t]$ for each time step.

Looking closely at Eq. (3), we can quickly see that a single physical platform that can produce the weight matrix W_{hh} would in principle suffice to implement the entire depth of the neural network. However, this requires that $W_{\text{hh}}[t]$ can be reconfigured fast enough, i.e., all its entries must be updated for each new time step t . This kind of “time-variable neural network” (see Fig. 2b) utilizes ideas similar to Neural ODEs [45] and has also been called “Time-varying Recurrent Neural Networks” [46]. In principle, we can even time-multiplex all the neurons within each layer l , reducing h to a scalar, further drastically lowering the number of necessary distinct physical elements, as shown in Folded-in-time Deep Neural Networks [47]. However, this requires additional trade-offs in terms of connectivity and implementation complexity, so in this manuscript we consider that $h[t]$ physically stores the state of an entire hidden layer.

Reconfiguring the network weights $W_{\text{hh}}[t]$ and bias terms $b[t]$ at each step [48, 49, 50, 51] is an effective approach for creating larger neural networks with fewer hardware components. Indeed, we should think of classical digital neural networks as heavily employing this strategy. The parameters and activations of digital neural networks are usually intermittently stored and loaded in the cache memory close to the processors. Thus, the matrix-vector products and updates for forward passes are in actuality calculated sequentially even in digital computers. Note, that this is only worthwhile, because digital computers can reconfigure themselves at the clock rate.

Many PNNs do not have the ability to reconfigure their parameters fast enough to use such a time-multiplexing strategy. The physical mechanisms used for training and setting the weight parameter values are typically slower compared to the dynamical time-scales of forward inference, as discussed in the Supplemental Information Section S2. Creating PNNs with quickly reconfigurable weights is indeed a promising avenue for the field [10, 11, 15, 39, 52, 53]. But for those PNNs with parameters that cannot be changed on single-pass time scales, we must consider alternative ways of time-multiplexing.

In the extreme case, where we cannot reconfigure the weights during inference at all in Eq. (3), we can only hope to re-use the same layer over and over:

$$h[t + 1] = f(W_{\text{hh}} h[t] + b), \quad (5)$$

which describes the case of $W_{\text{hh}} = \text{const}$ resulting in a conventional stateless RNN [54] (see Fig. 2c for a sketch). This choice does not limit the number of “layers” we can implement — we merely need to repeat the same operation over and over, if we so desire, although typical RNN language would not refer to the number of repetitions as layers. The number of trainable parameters is however limited to the dimensions of W_{hh} and b .

At this stage, one may think that these are the options available to a PNN — either parameters can be reconfigured fast, or they cannot. If, in line with realities of most PNNs, the parameters of the weight matrices are assumed to be fixed during forward-passes, does this imply our only choice is to implement a classical stateless RNN, or to pay the high hardware cost of having a separate hardware element for each layer? In fact, there is an additional class of time-multiplexed networks that lies conceptually in-between the stateless RNN of Eq. (5) and the fully time-variable DNN of Eq. (3). This is the idea behind the proposed ReLaX-Net architecture (see Fig. 2d for a sketch), which is explained in detail in the following section.

3 Reuse of Layers for eXpanding a Neural Network (ReLaX-Net)

We consider new ways for implementing a multilayer PNN to relax physical constraints in PNNs, while improving the performance. Specifically, we expand upon the idea of simple stateless RNNs as illustrated in Fig. 2c. The main conceptual hurdle, as identified in the previous section, is that we typically cannot assume that the weights $W_{\text{hh}}[t]$ and bias parameters $b[t]$ can be reconfigured quickly, making it infeasible to construct a neural network via layer-by-layer time-multiplexing (see Eq. (3) and Fig. 2b). Instead, under some reasonable assumptions, we can explore a neural network architectures that are still plausibly constructible with such restricted PNN hardware, but exceed stateless RNNs in hardware efficiency.

The main idea is the following: While the parameters $\theta_t = \{W_{\text{hh}}[t], b[t]\}$ of each physical layer themselves may be fixed, fast switches can still allow PNNs to be constructed flexibly from multiple fixed layers. For example, in the simplest case, we may assume two physically implemented weight matrices W_{hh}^0 and W_{hh}^1 . By chaining the first and second kind of weight matrix, we can create a non-trivial deep neural network, with a different functionality than a stateless RNN. These deep neural networks are described by a certain structure of tied-weights — certain layers sharing the same parameters — which allows us to explore a richer set of architectures.

ReLaX-Net architecture is a neural network with $L_{\text{T}} \in \mathbb{N}$ layers, described by the time evolution of the hidden state $h[t] \in \mathbb{R}^N$:

$$h[t+1] = \alpha h[t] + f(W_{\text{xh}}x[t] + W_{\text{hh}}[t]h[t] + b_{\text{h}}[t]), \quad (6)$$

where W_{xh} describes the input weights for input $x[t]$ and α is the strength of the residual connection, which is adopted for stable learning. Each time step t corresponds to one of the layers $t = \{0, 1, \dots, L_{\text{T}}\}$. The parameters of the hidden layers $\theta[t] =$

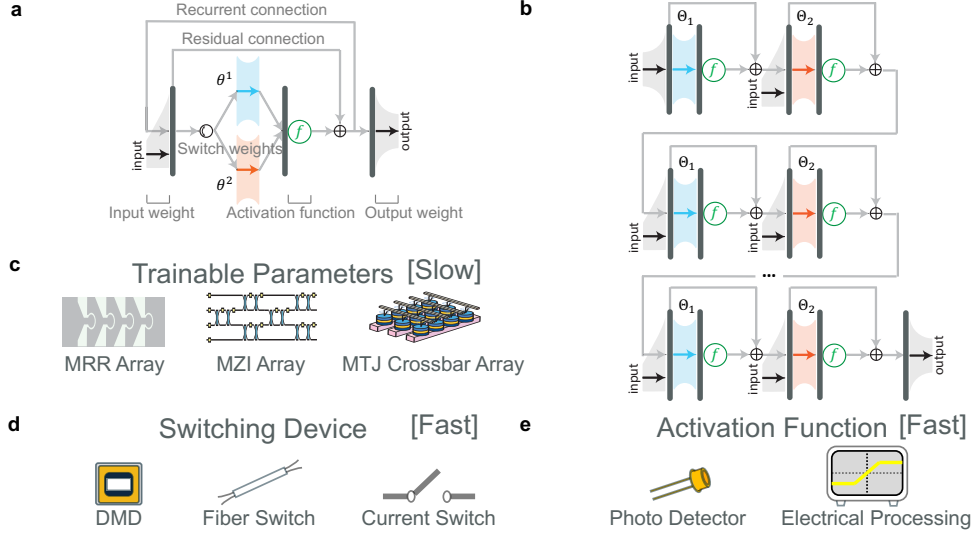


Fig. 3 Reuse of Layers for eXpanding a Neural Network (ReLaX-Net). **a**: The forward propagation switches between separate sets of hidden layers with different parameters $\theta = (W_{hh}, b_h)$, see Eq. (6). This enables the hardware-efficient reuse of many components while only requiring high-speed switches (parameter reconfiguration can happen at much slower speeds). **b**: If we consider how layers are chained temporally, this forms a deep neural network. The total depth is given by the number of repetitions L_T . **c**, **d**, **e**: Examples of proposed implementations for PNN components: **c**: Micro-Ring Resonator (MRR), Mach-Zehnder Interferometer (MZI) and Magnetic Tunnel Junctions (MTJ) Crossbar Arrays for trainable parameters; **d**: Digital Mirror Devices (DMD), Fiber Switches and Current Switches for switching devices ; **e**: Photo Detectors or Electrical Processing for the non-linear activation function.

$\{W_{hh}[t], b_h[t]\}$ change periodically as

$$\theta[t] = \begin{cases} \theta^1 & (t \bmod L_W \equiv 0) \\ \theta^2 & (t \bmod L_W \equiv 1) \\ \dots & \\ \theta^{L_W} & (t \bmod L_W \equiv L_W - 1) \end{cases} \quad (7)$$

with L_W being the number of different parameter sets for the hidden layers, i.e., weights and biases, which correspond to chaining weight matrices [55].

Figure 3 illustrates ReLaX-Net in the case of two periodically switched layers $L_W = 2$. For the most hardware-efficient implementations, the PNN should reuse as many elements as possible between layers (see Fig. 3a). This creates an effective deep neural network via time-multiplexing as shown in Fig. 3b. We only need to duplicate those physical elements that implement the trainable parameters θ^l . Common examples for those are Micro-Ring Resonator [11], Mach-Zehnder Interferometer [10] or Magnetic Tunnel Junction crossbar arrays [15] (see Fig. 3c). The nonlinear activation function (Fig. 3e) can be shared, which also ensures a high degree of uniformity between layers. ReLaX-Net expects the usage of fast electronic switches, such as those

shown in Fig. 3d. Many common PNN platforms should be able to use fast switching devices, such as Digital Mirror Device (DMD) [56] or optical fiber switches [57] in photonic systems. Importantly, it is only these fast switches that need to operate at the speed of the dynamic variables of the forward pass — all other elements can be considerably slower and parameters need to only be trainable on the time scales of training batches and epochs. For example, while ReLaX-Net application target systems typically take sub-microseconds for their reconfiguration [58], some researchers achieve even femtoseconds switching [57]. See the Supplemental Information Section S2 for details.

By changing the time-multiplexing steps L_T and number of unique physical parameter sets L_W , we can implement a variety of different setups, as shown in Fig. 4, where different colors indicate distinct parameters θ^l for the layers. In particular, the classical case of a stateless RNN is recovered by choosing $L_T > 1$ and $L_W = 1$ (see Fig. 4, left). Conversely, choosing $L_W = L_T$ would mean that no layers are re-used, and we instead have recreated a direct correspondence between hardware and model parameters. The novel hardware-efficient setups that we aim to explore involve all cases of $1 < L_W < L_T$, where at least some layers are reused, as shown on the right of Fig. 4.

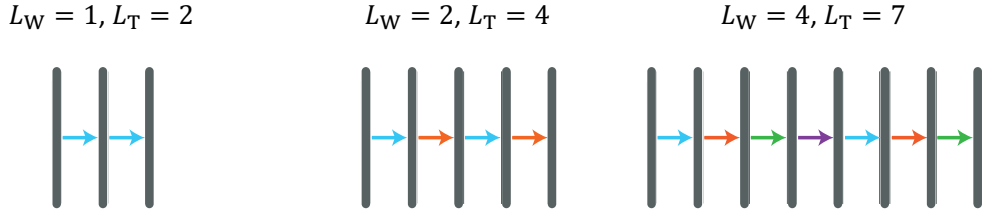


Fig. 4 Examples of ReLaX-Net. From left to right, the cases are: $(L_W, L_T) = (1, 2), (2, 4), (4, 7)$. The gray solid line represents the hidden states, while the colored arrows inbetween represent the parameters of the transformations (weights and biases). Shared colors indicate that parameters were reused, whereas differing colors indicate unique parameters. L_T corresponds to the number of layers and L_W corresponds to the number of distinct colors of the arrows, i.e., parameter sets.

To our knowledge, these architectures lying between RNNs and DNNs have not been discussed from a standpoint of hardware efficiency previously. We would be surprised to find that they had not been considered at all before, but ReLaX-net-like architectures are especially suitable for PNNs. As stated previously, in a digital computer, there is less justification for studying the $1 < L_W < L_T$ cases, i.e., reusing several layers. It simply is often tempting to untie the weights of all the layers and let gradient descent optimize each layer individually. Inside a digital computer, tying the weights in the manner proposed here might only yield a modest speed-up (mostly by reducing the memory footprint). For PNNs, however, the difference might be much more dramatic. In the following, we will benchmark the performance of ReLaX-net to act supply a baseline and compare it to existing DNN and RNN schemes.

4 ReLaX-Net performance on typical benchmark tasks

We perform numerical experiments to demonstrate how the switching affects the number of trainable parameters, and how ReLaX-Net scales in terms of hardware efficiency. In Subsection 4.1 we explore the scaling of the performance when going from a stateless RNN to a full DNN, where ReLaX-Net describes the cases in-between. Then, we investigate the general behavior of ReLaX-Net for various values of L_T and L_W and how the model benefits from the temporal repetition in Subsection 4.2. Finally, we investigate what choice of L_T and L_W are optimal under a fixed parameter budget in Subsection 4.3.

To evaluate ReLaX-Net generically, we use two different data sets. First, we test it on the Street View House Number (SVHN) [59] image classification task. (See Supplemental Information Section S3.8, S4, S5 for details.) Additionally, we also performed a simulation for a natural language processing (NLP) task. (See Supplemental Information Section S3.9, S6 for details.)

Unless otherwise specified, the following configurations were used: A ReLU activation function was employed to introduce nonlinearity, and the trainable parameters, except for α , were initialized using the Kaiming method [60]. The residual connection α is initialized to 1.0. For the SVHN task, data augmentation on the images was performed as described in Supplemental Information Section 3.8 to prevent overfitting to too minor features. We use 73257 images for training and 26032 test images, and the training was run for 900 epochs. Each image is a 32×32 RGB image containing a central digit to be classified.

For the NLP task, we applied the variational RNN dropout method [61], which is also described in the Supplemental Information Section 3.9. Our training corpus (Shakespearean plays) consists of 9044939 characters, of which 90% are used for training and 10% are used for testing. Before training and testing, character data are preprocessed as explained in Supplemental Information Section 3.9. We use single letters of the English alphabet and some basic symbols as tokens for a total set of 43 values, and the training was run for 200 epochs. We choose hidden state and weight sizes corresponding to existing PNN hardware. The hidden layers have 64 nodes for the SVHN task and 128 nodes for the NLP task. All results shown are for the test sets.

4.1 Benchmark task performance

First, Figure 5 shows the performance of our numerically simulated ReLaX-Net on the Street View House Number (SVHN) image classification task [59]. Here, the number of unique weights L_W is changed while the depth, i.e., number of time steps L_T is fixed (see Fig. 5b). We evaluate both the error rate of the image classification (blue line and dots in Fig. 5a). The gray dotted line shows the error rate and loss, respectively, of a corresponding stateless RNN. This is the limit of ReLaX-net when $L_W = 1$, as shown on the left of Fig. 5b. On the other end, when $L_W = L_T = 12$, the system effectively acts as a 12-layer MLP. Accordingly, we are especially interested in exploring the behavior of ReLaX-Net in the intermediate regime of $1 < L_W < L_T = 12$.

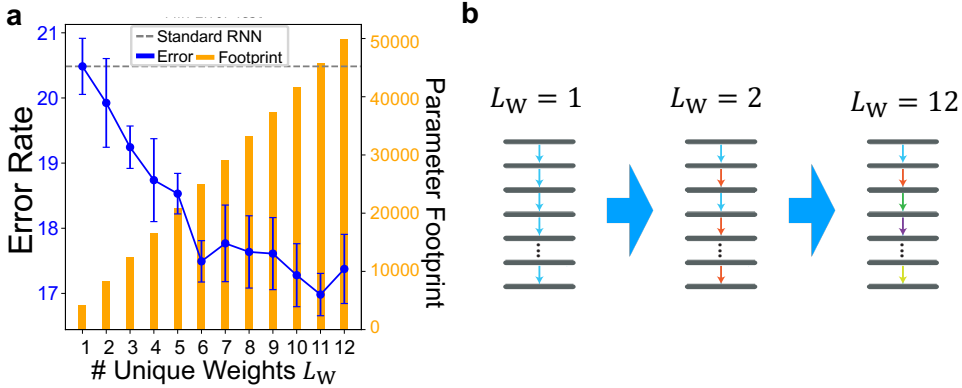


Fig. 5 ReLaX-Net performance on the SVHN image classification task. The number of unique weight matrices L_W is changed while keeping the number of layers $L_T = 12$ fixed. **a**: Error Rate and Parameter Footprint when varying L_W . Blue dots and lines show the Error Rate, and orange bars show the number of trainable parameters in the hidden layers, corresponding to the hardware footprint. The dashed line is the performance of the stateless RNN limit for $L_W = 1$. **b**: Illustration of ReLaX-Net architectures. Gray bars represent the hidden layers, and arrows indicate hidden weights. (Left) Reusing the same hidden weight. ($L_W = 1$) (Middle) Repeating two-weights. ($L_W = 2$) (Right) Reconfiguring at every time step. ($L_W = 12$) ReLaX-Net $L_W \geq 2$ cases are better than standard RNN $L_W = 1$ cases. Especially, with a few additional layers, ReLaX-Net can outperform standard RNNs.

The number of trainable parameters of the hidden layers (elements of W_{hh} and b_h) is shown in yellow and referred to on the secondary y-axis in Fig. 5a. This naturally increases linearly with L_W . Note that this count excludes input weights W_{xh} and output weights W_{yh} , which are often implemented using different hardware than the hidden layers. General trends remain the same even with random but non-trainable input layers and are shown in the following Subsection 4.2.

In Fig. 5a, the error rate decreases as the number of unique weight matrices L_W increases, which demonstrates the positive effect of increased parameter counts on image classification. The decrease is first steep and then flattens out, with a reverse hockey-stick shape. This shows that just a few additional sets of weights already provide a significant boost to the performance. The exact decline is a complex combination of several effects. Clearly, increasing the number of trainable parameters is expected to improve the performance, and clearly we expect this effect to be the strongest when going from $L_W = 1$ to 2. But as we will show in Subsection 4.2, the improvement of the performance seen in Fig. 5 is not purely caused by the increase in parameters, but also benefits from the repetition employed by ReLaX-Net.

Figure 6 shows the result on Natural Language Processing (NLP) (Shakespearean texts [62]) task. For this task, we use the fact that we can input $x[t]$ at each time step, inputting a different token in each layer. Here, the decline of the error (blue line in Fig. 6) is even steeper with L_W . Performance does not increase when L_W reaches around 6, which is likely caused by vanishing gradients. This is in spite of the fact that we already employ a simple residual connection (see Eq. (6)) and use careful initialization. This highlights that PNNs need to consider the lessons learned

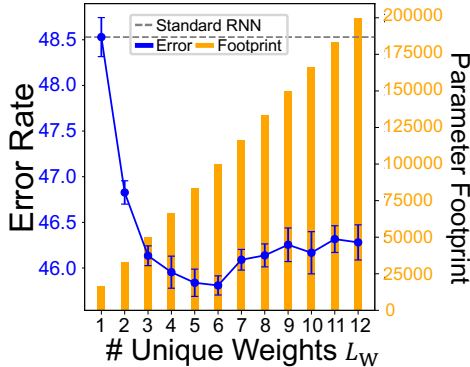


Fig. 6 ReLaX-Net performance on a natural language processing task. The number of unique weight matrices L_W is changed while keeping the number of layers $L_T = 12$ constant. Blue dots and lines show the Error Rate, and orange bars show the number of trainable parameters, corresponding to the hardware footprint. The gray dashed line is the performance of the stateless RNN limit for $L_W = 1$. Especially, with a few additional layers, ReLaX-Net can outperform standard RNNs.

the general deep learning community — a merely very deep multi-layer perceptron is not optimally utilizing its vast amount of parameters. Due to the reuse of layers in ReLaX-net, the architecture is more robust to vanishing gradients when $1 < L_W < L_T = 12$. The same layer appears, in general, multiple times, allowing the gradient over different layers to add up. This unique characteristic results in not only performance improvement when parameters increase, but also training stability and resilience to gradient explosion/vanishing. It is also better than the pure RNN case, because only repeating identical weights over and over is known to cause instability [63].

For both tasks, we can confirm that the performance for $L_W > 1$ consistently surpasses the $L_W = 1$ RNN case. These results confirm that ReLaX-Net achieves performance gains with only moderate modifications, supporting its feasibility for scalable physical implementations. We have also confirmed that these results are consistent when using a different nonlinear activation function, especially on SVHN classification, see the Supplementary Information Section S7 for details.

4.2 Importance of Repetition in ReLaX-Net

One of ReLaX-Net’s distinctive features is its controlled repetition of weights, bridging characteristics of both RNNs and DNNs. Specifically, being different from a multilayer perceptron (DNN), ReLaX-Net reuses some weights like a RNN. Here, we demonstrate how repetitive use of multiple weights affects the performance on ReLaX-Net. In Fig. 7, we vary the number of layers L_T when the number of distinct sets of weights L_W is kept. For generality, we conducted the investigation on different L_W values. Fig. 7 **a(b)** shows the example case when the number of unique weight matrices L_W is 2 (3). Both plots show that a few repetitions result in better performance than the non-repetition baseline (the gray dashed line). Notably, changing L_T does not change the number of trainable parameters - the performance gains are purely thanks to repeating weights, which also helps to make the network deeper (see the top of Fig. 7)

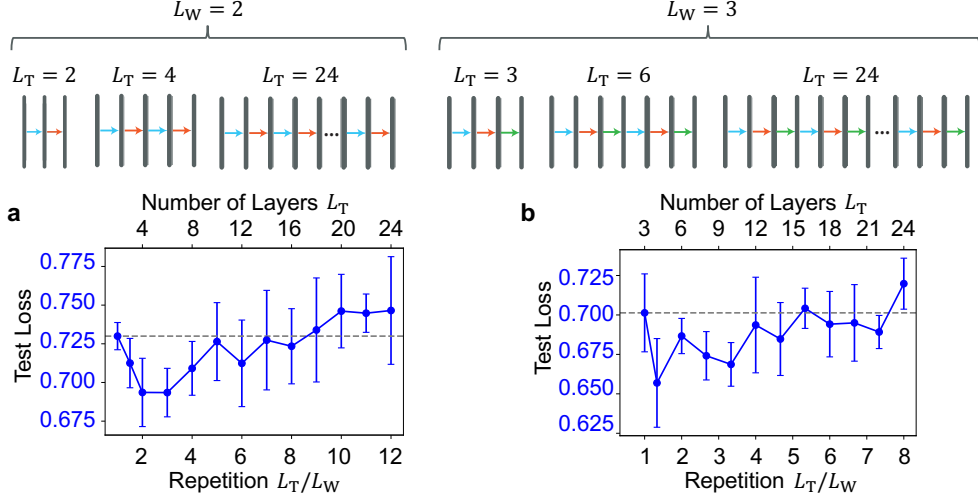


Fig. 7 ReLaX-Net performance on the SVHN image classification task with different time steps when the number of unique weight matrices L_W is fixed. **a**: when the number of unique weight matrices L_W is 2; **b**: when the number of unique weight matrices L_W is 3. Reuse of layers decreases the error rate for both cases.

ReLaX-Net combines the characteristics of standard RNNs and DNNs. By increasing the number of unique weight matrices L_W , ReLaX-Net can approach the high performance of DNNs. For example, without repetition, the error rate for $L_W = 3$ is better than that of the $L_W = 2$ case. On the other hand, by increasing the number of layers L_T , we also notice RNN-like characteristics. This includes the tendency for the performance to worsen eventually, if too many repetitions are used [64], as depicted in Fig. 7. In any specific PNN, it is therefore key for designing a high-performing ReLaX-Net to balance between DNN-like and RNN-like characteristics.

4.3 PNNs under a fixed parameter budget

Seeing the results of the previous section, one might be tempted to conclude the well-established fact that a deep neural network is, in many cases, much more powerful than a shallow one. In this sense, ReLaX-net emphasizes the inherent power of using multiple distinct layers, instead of just a single one. Therefore, one may wonder whether it is worth considering to *artificially* increase the set of distinct weights when building a PNN from various physical components. For example, one may be able to use the same lab space, or wafer space for an integrated chip, or temporal range for a time-multiplexed network, to either implement one large layer, or two smaller layers. Here we want to consider such a scenario and investigate the performance using a fixed parameter budget.

We choose a size of roughly 33000 trainable parameters, and divide these among L_W distinct weight matrices W_{hh} , as shown in Table 1. To isolate the effect we care for, we also use fixed random input parameters W_{xh} , as otherwise the implicit number of trainable parameters of the input layer would vary with L_W as well.

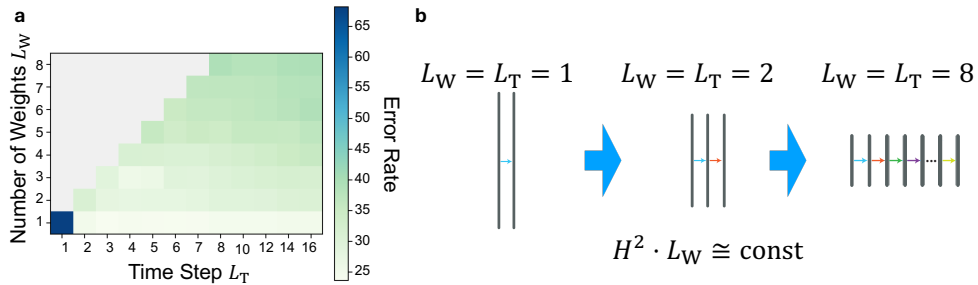


Fig. 8 ReLaX-Net performance heatmap on the SVHN classification when the total number of trainable parameters is fixed. **a**: Error. The number of distinct layers L_W is varied along the y-axis, while the number of temporal repetitions L_T is varied along the x-axis. **b**: The fixed parameter budget necessitates that as more distinct layers are added (larger L_W), these layers become smaller. Performance is the best for the widest layer $L_W = 1$ for the parameters tested here, see Table 1.

Figure 8 shows a 2D plot of the performance of ReLaX-Net on the SVHN image classification task under this fixed parameter budget. Here, we vary the number of unique weight matrices L_W on the y-axis and the number of layers L_T (temporal length) on the x-axis. Note that the parameter budget is independent of L_T , as this merely represents repeating previous layers. When L_W changes, it also changes the size of the hidden layers as per Table 1 (see Fig. 8b). Cases of $L_W > L_T$ are impossible and represented by gray cells.

As can be seen by the color code for the test error (Fig. 8a), the performance is best with $L_W = 1$ and $L_T > 1$. This corresponds to the case of a single, large layer, with a few repetitions.

These results indicate, that, at least in the tested cases, it is not worth to sacrifice the size of individual layers in order to increase the number of distinct layers in ReLaX-net. ReLaX-Net is beneficial when physical constraints, such as size or heat dissipation limits, are already setting the maximum size of each trainable layer in terms of the dimension of θ^l . But as Fig. 8 shows, halving the size of each layer, in order to increase the number of layers, does not increase the performance under the conditions we tested. Nevertheless, from the 2D-plots in Fig. 8 we can see that for each fixed L_W row, the best performance is typically achieved for $L_T > L_W$. i.e., when at least some layers are repeated, showcasing once more one of the main motivations for ReLaX-Net.

5 Discussion

We have discussed the importance and scaling of the number of trainable parameters for artificial neural networks, noting that many PNNs lag far behind in terms of scale. To address this issue, we propose a modified version of time-multiplexing, which only requires high-speed switches for the hardware, but allows the other elements, in particular the training of parameters, to operate with slower physical principles. The resultant architecture is called ReLaX-Net.

We test our results on an image classification and natural language benchmark task, demonstrating that switching between a small set of weights is an effective

approach to enhance performance. By balancing between the number of parameters and implementation cost, ReLaX-Net opens new pathways for scaling PNNs. Numerical experiments also emphasize the importance of preparing appropriate parameters, such as the number of time steps and the number of unique weight matrices for the ReLaX-Net configuration. The optimal values of L_W and L_T depend on the task and the available implementation resources. We present generic cases to make our results as broadly applicable as possible, but each individual PNN will have to consider additional details. We consider additional trade-offs for the parameters in the Supplemental Information Section S8.

Like all scaling approaches, ReLaX-Net requires the resource for extra weights to be implemented, but it does not need dynamic reconfiguration during inference. These multiple trainable weights are then switched between during inference. Surprisingly, “dividing” a large physical trainable layer into multiple smaller ones (to achieve a higher depth) is not worth the trade-off according to our numerical simulations.

In addition, it is worth noting that in the research field of machine learning, the related idea of weight sharing or weight tying has been explored in various fields and is commonly used in architectures like the Transformer [5]. Our results confirm and extend the knowledge of digital neural networks with weight-sharing, and ReLaX-Net reconsiders these principles with a view to the physical domain, offering a way to relax physical constraints to achieve practical physical computing systems.

Our particular choice of time-multiplexing — periodic switching of entire layers — is only the most basic among a potentially much larger class of partially time-multiplexed physical neural networks. By explicitly separating the time scales of learning — associated with trainable parameters and weight updates etc. — from those of inference (forward passes, input, output), ReLaX-Net establishes a practical framework for resource-efficient physical computing. Digital computers are, after all, implementing both the forward pass as well as the storing of weights and parameters using the same hardware. And as discussed before, we should regard them as highly time-multiplexed computers — in principle, a single processor can calculate the entire forward path sequentially while loading and unloading memory. Different from them, ReLaX-Net clearly separates the hardware needs of these two time-scales — learning and inference — from a PNN-centric perspective, while also preserving some of the advantages of efficient hardware re-use. Future works should address how PNNs can systematically find the optimal switching patterns given their particular hardware needs and timescales.

One of the next crucial steps for the future development of ReLaX-Net is the experimental realization in PNN platforms. This framework is compatible with various substrates, including photonic and spintronic systems, where slow tunable weights and fast switching devices coexist. Future work will focus on developing concrete implementation structures and verifying real-time weight switching in these hardware environments. In particular, integrating high-speed optical or electrical switches with slower trainable components such as Micro-Ring Resonator weight banks, Mach-Zehnder Interferometer circuits, or Magnetic Tunnel Junction crossbar arrays could experimentally demonstrate the time-multiplexed computation proposed in this study. See Supplemental Information Section S2 for details. With these implementations,

ReLaX-Net can present a pathway to scalable and energy-efficient physical computing systems in the near future era of intermediate size PNNs.

Data availability

All data generated during and code used for this work will be available from the corresponding author upon reasonable request.

References

- [1] Yann LeCun, Yoshua Bengio, and Geoffrey Hinton. Deep learning. *nature*, 521(7553):436–444, 2015.
- [2] Karen Simonyan and Andrew Zisserman. Very deep convolutional networks for large-scale image recognition. *arXiv preprint arXiv:1409.1556*, 2014.
- [3] Joseph Redmon, Santosh Divvala, Ross Girshick, and Ali Farhadi. You only look once: Unified, real-time object detection. In *Proceedings of the IEEE conference on computer vision and pattern recognition*, pages 779–788, 2016.
- [4] Kaiming He, Xiangyu Zhang, Shaoqing Ren, and Jian Sun. Deep residual learning for image recognition. In *Proceedings of the IEEE conference on computer vision and pattern recognition*, pages 770–778, 2016.
- [5] Ashish Vaswani, Noam Shazeer, Niki Parmar, Jakob Uszkoreit, Llion Jones, Aidan N Gomez, Lukasz Kaiser, and Illia Polosukhin. Attention is all you need. *Advances in neural information processing systems*, 30, 2017.
- [6] Jacob Devlin, Ming-Wei Chang, Kenton Lee, and Kristina Toutanova. Bert: Pre-training of deep bidirectional transformers for language understanding. In *Proceedings of the 2019 conference of the North American chapter of the association for computational linguistics: human language technologies, volume 1 (long and short papers)*, pages 4171–4186, 2019.
- [7] Gordon Wetzstein, Aydogan Ozcan, Sylvain Gigan, Shanhui Fan, Dirk Englund, Marin Soljačić, Cornelia Denz, David AB Miller, and Demetri Psaltis. Inference in artificial intelligence with deep optics and photonics. *Nature*, 588(7836):39–47, 2020.
- [8] Lennert Appeltant, Miguel Cornelles Soriano, Guy Van der Sande, Jan Danckaert, Serge Massar, Joni Dambre, Benjamin Schrauwen, Claudio R Mirasso, and Ingo Fischer. Information processing using a single dynamical node as complex system. *Nature communications*, 2(1):468, 2011.
- [9] Kristof Vandoorne, Pauline Mechet, Thomas Van Vaerenbergh, Martin Fiers, Geert Morthier, David Verstraeten, Benjamin Schrauwen, Joni Dambre, and Peter Bienstman. Experimental demonstration of reservoir computing on a silicon photonics chip. *Nature communications*, 5(1):3541, 2014.
- [10] Yichen Shen, Nicholas C Harris, Scott Skirlo, Mihika Prabhu, Tom Baehr-Jones, Michael Hochberg, Xin Sun, Shijie Zhao, Hugo Larochelle, Dirk Englund, et al. Deep learning with coherent nanophotonic circuits. *Nature photonics*, 11(7):441–446, 2017.

- [11] Alexander N Tait, Thomas Ferreira De Lima, Ellen Zhou, Allie X Wu, Mitchell A Nahmias, Bhavin J Shastri, and Paul R Prucnal. Neuromorphic photonic networks using silicon photonic weight banks. *Scientific reports*, 7(1):7430, 2017.
- [12] Julian Bueno, Sheler Maktoobi, Luc Froehly, Ingo Fischer, Maxime Jacquot, Laurent Larger, and Daniel Brunner. Reinforcement learning in a large-scale photonic recurrent neural network. *Optica*, 5(6):756–760, 2018.
- [13] Xing Lin, Yair Rivenson, Nezih T Yardimci, Muhammed Veli, Yi Luo, Mona Jarrahi, and Aydogan Ozcan. All-optical machine learning using diffractive deep neural networks. *Science*, 361(6406):1004–1008, 2018.
- [14] Carl Ramey. Silicon photonics for artificial intelligence acceleration: Hotchips 32. In *2020 IEEE hot chips 32 symposium (HCS)*, pages 1–26. IEEE Computer Society, 2020.
- [15] Seungchul Jung, Hyungwoo Lee, Sungmeen Myung, Hyunsoo Kim, Seung Keun Yoon, Soon-Wan Kwon, Yongmin Ju, Minje Kim, Wooseok Yi, Shinhee Han, et al. A crossbar array of magnetoresistive memory devices for in-memory computing. *Nature*, 601(7892):211–216, 2022.
- [16] Logan G. Wright, Tatsuhiro Onodera, Martin M. Stein, Tianyu Wang, Darren T. Schachter, Zoey Hu, and Peter L. McMahon. Deep physical neural networks trained with backpropagation. *Nature*, 601:549–555, 2022.
- [17] Jacob Torrejon, Mikael Riou, Fabio AP Araujo, Shunsuke Tsunegi, Guru Khalsa, Damien Querlioz, Paolo Bortolotti, Vincent Cros, Kay Yakushiji, Akio Fukushima, et al. Neuromorphic computing with nanoscale spintronic oscillators. *Nature*, 547(7664):428–431, 2017.
- [18] Erwan Plouet, Dédalo Sanz Hernández, Aymeric Vecchiola, Julie Grollier, and Alice Mizrahi. Training a multilayer dynamical spintronic network with standard machine-learning tools to perform time-series classification. *Physical Review Applied*, 23(3):034051, mar 2025.
- [19] Miguel Romera, Philippe Talatchian, Sumito Tsunegi, Flavio Abreu Araujo, Vincent Cros, Paolo Bortolotti, Juan Trastoy, Kay Yakushiji, Akio Fukushima, Hitoshi Kubota, et al. Vowel recognition with four coupled spin-torque nanos oscillators. *Nature*, 563(7730):230–234, 2018.
- [20] Juan Manuel Parrilla-Gutierrez, Abhishek Sharma, Soichiro Tsuda, Geoffrey JT Cooper, Gerardo Aragon-Camarasa, Kevin Donkers, and Leroy Cronin. A programmable chemical computer with memory and pattern recognition. *Nature communications*, 11(1):1442, 2020.
- [21] Shaohua Kan, Kohei Nakajima, Tetsuya Asai, and Megumi Akai-Kasaya. Physical implementation of reservoir computing through electrochemical reaction. *Advanced Science*, 9(6):2104076, 2022.
- [22] Alex Krizhevsky, Ilya Sutskever, and Geoffrey E Hinton. Imagenet classification with deep convolutional neural networks. In *Advances in Neural Information Processing Systems*, volume 25, pages 1097–1105, 2012.
- [23] Alec Radford, Karthik Narasimhan, Tim Salimans, Ilya Sutskever, et al. Improving language understanding by generative pre-training. 2018.
- [24] Mohammad Shoeybi, Mostofa Patwary, Raul Puri, Patrick LeGresley, Jared Casper, and Bryan Catanzaro. Megatron-lm: Training multi-billion parameter

- language models using model parallelism. *arXiv preprint arXiv:1909.08053*, 2019.
- [25] Alec Radford, Jeffrey Wu, Rewon Child, David Luan, Dario Amodei, Ilya Sutskever, et al. Language models are unsupervised multitask learners. *OpenAI blog*, 1(8):9, 2019.
- [26] Colin Raffel, Noam Shazeer, Adam Roberts, Katherine Lee, Sharan Narang, Michael Matena, Yanqi Zhou, Wei Li, and Peter J Liu. Exploring the limits of transfer learning with a unified text-to-text transformer. *Journal of machine learning research*, 21(140):1–67, 2020.
- [27] Tom B. Brown, Benjamin Mann, Nick Ryder, Melanie Subbiah, Jared Kaplan, Prafulla Dhariwal, Arvind Neelakantan, Pranav Shyam, Girish Sastry, Amanda Askell, et al. Language models are few-shot learners. In *Advances in Neural Information Processing Systems*, volume 33, pages 1877–1901, 2020.
- [28] William Fedus, Barret Zoph, and Noam Shazeer. Switch transformers: Scaling to trillion parameter models with simple and efficient sparsity. *Journal of Machine Learning Research*, 23(120):1–39, 2022.
- [29] Aakanksha Chowdhery, Sharan Narang, Jacob Devlin, Maarten Bosma, Gaurav Mishra, Adam Roberts, Paul Barham, Hyung Won Chung, Charles Sutton, Sebastian Gehrmann, et al. Palm: Scaling language modeling with pathways. *Journal of Machine Learning Research*, 24(240):1–113, 2023.
- [30] Johannes Feldmann, Nathan Youngblood, C David Wright, Harish Bhaskaran, and Wolfram HP Pernice. All-optical spiking neurosynaptic networks with self-learning capabilities. *Nature*, 569(7755):208–214, 2019.
- [31] Peng Yao, Huaqiang Wu, Bin Gao, Jianshi Tang, Qingtian Zhang, Wenqiang Zhang, J Joshua Yang, and He Qian. Fully hardware-implemented memristor convolutional neural network. *Nature*, 577(7792):641–646, 2020.
- [32] Jie Sun, Wuhaoyang, Tianyi Zheng, Xingyin Xiong, Yunfei Liu, Zheng Wang, Zhitian Li, and Xudong Zou. Novel nondelay-based reservoir computing with a single micromechanical nonlinear resonator for high-efficiency information processing. *Microsystems & Nanoengineering*, 7(1):83, 2021.
- [33] Takahiro Inagaki, Kensuke Inaba, Timothée Leleu, Toshimori Honjo, Takuya Ikuta, Koji Enbutsu, Takeshi Umeki, Ryoichi Kasahara, Kazuyuki Aihara, and Hiroki Takesue. Collective and synchronous dynamics of photonic spiking neurons. *Nature communications*, 12(1):2325, 2021.
- [34] Jared Kaplan, Sam McCandlish, Tom Henighan, Tom B Brown, Benjamin Chess, Rewon Child, Scott Gray, Alec Radford, Jeffrey Wu, and Dario Amodei. Scaling laws for neural language models. *arXiv preprint arXiv:2001.08361*, 2020.
- [35] Pablo Villalobos, Jaime Sevilla, Tamay Besiroglu, Lennart Heim, Anson Ho, and Marius Hobbhahn. Machine learning model sizes and the parameter gap. *arXiv preprint arXiv:2207.02852*, 2022.
- [36] Jingtian Hu, Deniz Mengü, Dimitrios C Tzarouchis, Brian Edwards, Nader Engheta, and Aydogan Ozcan. Diffractive optical computing in free space. *Nature Communications*, 15(1):1525, 2024.
- [37] MA Al-Qadasi, L Chrostowski, BJ Shastri, and S Shekhar. Scaling up silicon photonic-based accelerators: Challenges and opportunities. *APL Photonics*, 7(2), 2022.

- [38] Stefano Biasi, Riccardo Franchi, Davide Bazzanella, and Lorenzo Pavesi. On the effect of the thermal cross-talk in a photonic feed-forward neural network based on silicon microresonators. *Frontiers in Physics*, 10:1093191, 2022.
- [39] Julie Grollier, Damien Querlioz, Kerem Y Camsari, Karin Everschor-Sitte, Shun-suke Fukami, and Mark D Stiles. Neuromorphic spintronics. *Nature electronics*, 3(7):360–370, 2020.
- [40] Peter L McMahon. The physics of optical computing. *Nature Reviews Physics*, 5(12):717–734, 2023.
- [41] Yann LeCun, Bernhard Boser, John Denker, Donnie Henderson, Richard Howard, Wayne Hubbard, and Lawrence Jackel. Handwritten digit recognition with a back-propagation network. *Advances in neural information processing systems*, 2, 1989.
- [42] Pierre Baldi and Kurt Hornik. Neural networks and principal component analysis: Learning from examples without local minima. *Neural Networks*, 2(1):53–58, 1989.
- [43] Oscar Chang and Hod Lipson. Balanced and deterministic weight-sharing helps network performance. In *International Conference on Artificial Neural Networks*, pages 41–50, 2018.
- [44] John Preskill. Quantum computing in the nisq era and beyond. *Quantum*, 2:79, 2018.
- [45] Ricky T. Q. Chen, Yulia Rubanova, Jesse Bettencourt, and David Duvenaud. Neural ordinary differential equations. In *Advances in Neural Information Processing Systems (NeurIPS)*, volume 31, 2018.
- [46] Yongxu Zhang, Catalin Mitelut, David J Arpin, David Vaillancourt, Timothy Murphy, and Shreya Saxena. Behavioral classification of sequential neural activity using time varying recurrent neural networks. *IEEE Transactions on Neural Systems and Rehabilitation Engineering*, 2025.
- [47] Florian Stelzer, André Röhm, Raul Vicente, Ingo Fischer, and Serhiy Yanchuk. Deep neural networks using a single neuron: folded-in-time architecture using feedback-modulated delay loops. *Nature communications*, 12(1):5164, 2021.
- [48] David Ha, Andrew Dai, and Quoc V Le. Hypernetworks. *arXiv preprint arXiv:1609.09106*, 2016.
- [49] Tyler W Hughes, Ian AD Williamson, Momchil Minkov, and Shanhui Fan. Wave physics as an analog recurrent neural network. *Science advances*, 5(12):eaay6946, 2019.
- [50] Xu Jia, Bert De Brabandere, Tinne Tuytelaars, and Luc V Gool. Dynamic filter networks. *Advances in neural information processing systems*, 29, 2016.
- [51] Jimmy Ba, Geoffrey E Hinton, Volodymyr Mnih, Joel Z Leibo, and Catalin Ionescu. Using fast weights to attend to the recent past. *Advances in neural information processing systems*, 29, 2016.
- [52] Alexander N Tait, Hasitha Jayatilleka, Thomas Ferreira De Lima, Philip Y Ma, Mitchell A Nahmias, Bhavin J Shastri, Sudip Shekhar, Lukas Chrostowski, and Paul R Prucnal. Feedback control for microring weight banks. *Optics express*, 26(20):26422–26443, 2018.
- [53] Daniel Pérez-López and Luis Torrijos-Morán. Large-scale photonic processors

- and their applications. *npj Nanophotonics*, 2(1):32, 2025.
- [54] Alex Graves. Generating sequences with recurrent neural networks. *arXiv preprint arXiv:1308.0850*, 2013.
 - [55] Samuel S Schoenholz, Jeffrey Pennington, and Jascha Sohl-Dickstein. A correspondence between random neural networks and statistical field theory. *arXiv preprint arXiv:1710.06570*, 2017.
 - [56] Larry J Hornbeck. Digital light processing and mems: timely convergence for a bright future. *Proceedings of SPIE*, 2639:2–14, 1997.
 - [57] Stephen R Friberg, Andrew M Weiner, YARON Silberberg, BRUNO G Sfez, and PS Smith. Femotosecond switching in a dual-core-fiber nonlinear coupler. *Optics Letters*, 13(10):904–906, 1988.
 - [58] Wim Bogaerts, Peter De Heyn, Thomas Van Vaerenbergh, Katrien De Vos, Shankar Kumar Selvaraja, Tom Claes, Pieter Dumon, Peter Bienstman, Dries Van Thourhout, and Roel Baets. Silicon microring resonators. *Laser & photonics reviews*, 6(1):47–73, 2012.
 - [59] Yuval Netzer, Tao Wang, Adam Coates, Alessandro Bissacco, Baolin Wu, Andrew Y Ng, et al. Reading digits in natural images with unsupervised feature learning. In *NIPS workshop on deep learning and unsupervised feature learning*, volume 2011, page 4. Granada, 2011.
 - [60] Kaiming He, Xiangyu Zhang, Shaoqing Ren, and Jian Sun. Delving deep into rectifiers: Surpassing human-level performance on imagenet classification. In *Proceedings of the IEEE international conference on computer vision*, pages 1026–1034, 2015.
 - [61] Yariv Gal and Zoubin Ghahramani. A theoretically grounded application of dropout in recurrent neural networks. *Advances in neural information processing systems*, 29, 2016.
 - [62] William Shakespeare. Shakespeare’s plays, sonnets and poems from the folger shakespeare. <https://folger.edu/explore/shakespeares-works/all-works>, n.d. Accessed: 2025-06-10.
 - [63] Razvan Pascanu, Tomas Mikolov, and Yoshua Bengio. On the difficulty of training recurrent neural networks. In *International conference on machine learning*, pages 1310–1318. Pmlr, 2013.
 - [64] Yoshua Bengio, Patrice Simard, and Paolo Frasconi. Learning long-term dependencies with gradient descent is difficult. *IEEE transactions on neural networks*, 5(2):157–166, 1994.
 - [65] Herbert Jaeger, Beatriz Noheda, and Wilfred G. van der Wiel. Toward a formal theory for computing machines made out of whatever physics offers. *Nature Communications*, 14(1):4911, 2023.
 - [66] Joni Dambre, David Verstraeten, Benjamin Schrauwen, and Serge Massar. Information processing capacity of dynamical systems. *Scientific reports*, 2(1):514, 2012.
 - [67] Guido F Montúfar, Razvan Pascanu, Kyunghyun Cho, and Yoshua Bengio. On the number of linear regions of deep neural networks. In *Advances in neural information processing systems*, volume 27, 2014.
 - [68] Diederik P Kingma. Adam: A method for stochastic optimization. *arXiv preprint*

- arXiv:1412.6980*, 2014.
- [69] Mitsumasa Nakajima, Katsuma Inoue, Kenji Tanaka, Yasuo Kuniyoshi, Toshikazu Hashimoto, and Kohei Nakajima. Physical deep learning with biologically inspired training method: gradient-free approach for physical hardware. *Nature Communications*, 13(1):7847, 2022.
 - [70] Satoshi Sunada, Tomoaki Niiyama, Kazutaka Kanno, Rin Nogami, André Röhm, Takato Awano, and Atsushi Uchida. Blending optimal control and biologically plausible learning for noise-robust physical neural networks. *Phys. Rev. Lett.*, 134:017301, Jan 2025.
 - [71] Boris T. Polyak. Some methods of speeding up the convergence of iteration methods. *USSR Computational Mathematics and Mathematical Physics*, 4(5):1–17, 1964.
 - [72] Geoffrey Hinton. Lecture 6e: Rmsprop — divide the gradient by a running average of its recent magnitude. Coursera: Neural Networks for Machine Learning, 2012. http://www.cs.toronto.edu/~tijmen/csc321/slides/lecture_slides_lec6.pdf.
 - [73] Yann LeCun, Léon Bottou, Yoshua Bengio, and Patrick Haffner. Gradient-based learning applied to document recognition. *Proceedings of the IEEE*, 86(11):2278–2324, 1998.
 - [74] Junhe Zhou, Qiqi Wang, and Chenweng Huang. Recurrent diffractive deep neural networks. *Optics Express*, 32(27):48093–48104, 2024.

Acknowledgements

We thank Felix Köster for fruitful feedback and discussions. This study was supported in part by a Grant-in-Aid for Transformative Research Areas (A) (JP22H05197), a Grant-in-Aid for JSPS Fellows (JP24KJ0868), Grant-in-Aid for Exploratory Research (JP25K22227), JST-ALCA-Next (JPMJAN25F1), JST FOREST Program (JPMJFR2448) and SECOM Science and Technology Foundation.

Author contributions

A.R. and K.T. conceived the project and methods. K.T. performed the numerical experiments. K.T. and A.R. wrote the manuscript. T.M. supported investigating and editing. R.H. supervised the project.

Competing interests

All authors declare no competing interests.

Tables

Table 1 The number of hidden nodes used in Fig. 8. Here, the trainable parameters consist of the network weights W_{hh} and bias terms b_h . This excludes the input-hidden network W_{xh} , hidden-output network W_{hy} and residual parameters α . Note: Total parameter counts fluctuate because the dimension of hidden nodes needs to be an integer.

# different layers L_W	1	2	3	4	5	6	7	8
hidden nodes per layer H	192	128	104	91	80	73	68	64
# trainable parameters	37057	32897	32761	33489	32401	32413	32845	33281

Appendix A Parameter counts of existing digital and physical neural networks

In Section 1 of the main manuscript, we talked about the importance of the number of trainable parameters for machine learning. Here, we provide the sources that were used in the creation of Fig. 1.

Table A1 — The Number of Trainable Parameters Shown in Fig. 1. The numbers of parameters shown here are based on what the original papers claim or our reasonable estimate of the system from information they supply.

	Architecture	Model	Year	Parameters
Electronic Computers		AlexNet [22]	2012	60,000,000
		VGG-19 [2]	2014	144,000,000
		GPT-1 [23]	2018	117,000,000
		BERT-Large [6]	2019	340,000,000
		Megatron-LM [24]	2019	8,300,000,000
		GPT-2 [25]	2020	1,500,000,000
		T5-11B [26]	2020	11,000,000,000
		GPT-3 [27]	2020	175,000,000,000
		Switch Transformer [28]	2022	1,600,000,000,000
		PaLM [29]	2023	540,000,000,000
PNN	Free Space Optics	Photonic RC [12]	2018	2,025
		D ² NN [13]	2018	450,000
		PAT [16]	2022	50,568
	Fiber Optics	Optoelectric RC [8]	2011	400
	Photonics on Chip	Integrated Photonic RC [9]	2014	16
		Nanophotonic Neural Network [10]	2017	112
		Micro-Ring Resonator (MRR) RNN [11]	2017	576
		Mars [14]	2020	4,096
	Hybrid	DOPO Network [33]	2021	57,600
	Spintronics	Spin-Torque Oscillator RC [17]	2017	400
		Coupled Spin Oscillator Network [19]	2018	30
		MRAM Crossbar Array [15]	2022	4,096
	MEMS	MEMS Nonlinear Resonator RC [32]	2021	440
	Chemitronics	Chemical Autoencoder [20]	2020	100
		Electrochemical RC [21]	2022	112
Memristor	Phase-Change Memory DNN [31]	2020	24,336	

First, we discuss how we obtained the parameter information of models for digital electronic computers. All parameter counts are based on publications by the respective designers of the networks themselves, and we have not included networks for which

we cannot find official sizes. Note that this excludes some of the most advanced Large Language Models (LLMs), which are most likely the largest systems, meaning that the true gap between Physical Neural Networks (PNNs) and digital neural networks might be even larger than shown. For AlexNet, the authors report that their model has 60 million parameters [22]. For the VGG19 paper [2], their model was reported to have 144 million parameters. The GPT-1 paper reports that the GPT-1 model has 117 million trainable parameters [23], including 31 million from embedding, 85 million from 12 Transformer blocks [5] and 0.5 million in LayerNorms and positional embedding. The authors of BERT-Large report that their model has 340 million parameters [6]. Megatron-LM has been described in the paper to have 8.3 billion parameters [24]. For GPT-2, OpenAI researchers reported that they have achieved a 1.5 billion parameters model [25]. The T5-11B researchers trained a 11 billion parameter model according to the main paper [26]. GPT-3 is reported as having 175 billion trainable parameters [27]. In the development of the Switch Transformer, researchers designed it to have 1.6 trillion parameters [28]. The PaLM model was trained with 540 billion parameters [29].

The estimation of parameters in PNN models can sometimes be more difficult. We have executed as much diligence as possible, but not all systems are straightforwardly interpretable. Here, we explain the source of the reported number of parameters of each PNN model. Note that all PNN systems that we cite require electronic supporting components. In this sense, they are hybrid systems. Supplementary Table A1 lists the PNNs and their sizes, where we have categorized the PNNs based on their primary physical mechanism. Note that, crucially, we do not distinguish between different levels of noise or resolution, e.g., systems using 4-bit vs 8-bit or 10-bit resolution in their trainable parameters are counted the same way. We do not believe that this is necessarily always justified, but in the absence of a coherent theory of physical computing [65], we will treat all these parameters as equivalent for now.

In Reservoir Computing (RC), the only trainable part is the output weight matrix. This means that the number of trainable parameters depends on the output dimension of the reservoir. Assuming a scalar variable per reservoir node, the number of parameters equals the number of reservoir nodes. Crucially, it is known that the computing capability of a RC is decided by the number of nodes [66]. The number of parameters of the RC systems in Supplementary Table A1 were taken from the following references: A Photonic RC with 2025 nodes [12], an optoelectric RC with 400 virtual nodes [8], an integrated photonics RC with 16 nodes [9], a Spin-Torque Oscillator RC with 400 nodes [17], a MEMS Nonlinear Resonator RC with 440 nodes [32] and an electrochemical RC with 112 nodes [21].

For the Diffractive Deep Neural Network (D²NN), a neuron corresponds to a point of a diffractive layer with a phase-only transmission coefficient, which is learnable. Accordingly, the number of trainable parameters corresponds to this number of neurons. The paper cited implements 0.45 million neurons in the system [13], one of the largest size PNN demonstrations to this day. Physical Aware Training (PAT) [16] is not limited to photonics, but the largest system in the original paper used photonics and achieved 50568 parameters. The shown Nanophotonic Neural Network had 56

Mach-Zehnder Interferometers [10], where each of them had 2 parameters (an internal and external phase) for a total of 112 trainable parameters. For the Micro-Ring Resonator (MRR) RNNs, a total of 576 MRR weights are used [11]. “Mars” by Lightmatter can achieve 64×64 matrix multiplications, implying that the system has 4096 parameters [14]. The parameters of the DOPO Network are implemented in a separate FPGA, and the number of learnable values is 57600 [33]. For the Coupled Spin Oscillator Network, 4 oscillators are achieved, with each of them having a bias current, which is the trainable part. In addition, there are 26 parameters in input weights as software components, for a total of 30 parameters [19]. In the Magnetoresistive Random-Access Memory (MRAM) Crossbar Array system, the researchers use a 64×64 crossbar array, and each component is trainable, resulting in 4096 parameters [15]. The chemical autoencoder has 25 independent BZ reaction chemical cells, which can be considered as 25 parameters [20]. Finally, the phase change memory DNN has 156×156 array [31], and it holds 24336 parameters.

Appendix B Timescales of training physical parameters in PNNs

As we discussed in the main text, the advantage of ReLaX-Net arises from the fast reconfiguration using simple devices such as switches. In this section, we provide additional information on the reconfiguration time for the existing PNN architectures and clarify the advantage of ReLaX-Net.

One of the promising ReLaX-Net application targets is a Micro-Ring Resonator (MRR) weight bank system [11]. In that system, the parameters of the MRR are changed by adjusting the temperature of its components [52]. Depending on conditions (e.g., required accuracy), weight reconfiguration using thermo-optic effects typically requires sub-microseconds [58], which is slow compared to the fast dynamic timescales of optical setups [56, 57]. Thus, when applying this system to a time variable neural network, the computation speed is dominated by the thermo-optic effect, which ReLaX-Net can avoid by switching.

Another candidate is a Mach-Zehnder Interferometer (MZI) based computing system [10], which often also utilizes the thermo-optic effect for its weight reconfiguration. Consequently, the speed of the tuning system is limited to the same time scale as the MRR system. So, by switching the MZI weight matrices, ReLaX-Net enables the system to achieve different weights dynamically at a higher frequency.

PNNs using Magnetic Tunnel Junction (MTJ) crossbar arrays [15] also represents a potential platform for ReLaX-Net. In their 64×64 MTJ system, the total reconfiguration time for the entire matrix is on the order of tens of microseconds. By incorporating switching in its electronic components, ReLaX-Net is also applicable to non-photonic PNNs and helps it achieve a time variable neural network.

Similarly, for PNNs whose matrix multiplication components operate slowly, ReLaX-Net can be implemented with additional fast components. This modest hardware requirement constitutes one of the key advantages and defining features of the ReLaX-Net framework.

Appendix C Principles of ReLaX-Net

In this section, we describe the Reuse of Layers for eXpanding a Neural Network (ReLaX-Net) and explain its practical advantages in implementing PNNs. The following subsections detail each component of our method.

C.1 Intuition

Switching network weights across time steps can increase the number of parameters in the RNN. For example, doubling the number of distinct weight matrices used in the recurrent loop effectively doubles the number of parameters, even without increasing the width of the layers. Simultaneously, this flipping mechanism introduces a deep computational structure composed of different network connections. Stacking networks that have different connections is widely known to improve representation power even with limited parameters [67]. Furthermore, from a hardware perspective, switching network weights may be significantly easier than duplicating the full network structures, particularly in the context of PNNs, where component size and reconfigurability are the key limitations.

The ReLaX-Net thus represents a middle ground between a standard RNN and a fully dynamic time-variable neural network, where its weights change over time as Supplementary Table C2 shows. As such, ReLaX-Net offers a practical and scalable solution for enhancing neural network expressivity while maintaining feasibility in physical implementation.

Table C2 — **Comparison among RNNs.** ReLaX-Net exists between a standard RNN and a time variable Neural Network.

	standard RNN	ReLaX-Net	time variable Neural Network
input/output weight	fixed	fixed	fixed
network weight	fixed	periodic switching	dynamical switching

C.2 Back-Propagation Through Time (BPTT)

In supervised machine learning, the training dataset consists of pairs of examples and targets $\{(x^k, y_{\text{target}}^k)\}_{k=1}^{N_{\text{batch}}}$, where N_{batch} is the batch size. During training, the goal is to obtain parameters of the network that maps any given example x^k to an output (prediction) \hat{y}^k that is as close as possible to the desired target y_{target}^k . In gradient-based optimization, this objective is achieved by minimizing a loss function L_{batch} over the dataset.

$$L_{\text{batch}} = \frac{1}{N_{\text{batch}}} \sum_k L^k \quad (\text{C1})$$

where $L^k = l(y_{\text{target}}^k, \hat{y}^k)$ is the loss on the k -th data and l denotes the chosen loss function. In our experiments, we use the cross-entropy loss l , which is explained in detail in subsection C.3.

Once the loss gradient with respect to model parameters is computed, parameters can be updated using any gradient descent-based optimizer. In our study, we use the Adam optimizer [68], which is introduced in subsection C.4, with a learning rate of 0.001.

To train ReLaX-Net, we apply Backpropagation Through Time (BPTT), which accounts for dependencies across time steps. BPTT computes the gradient of the loss with respect to the parameters $\phi = (\alpha, W_{\text{xh}}, W_{\text{hh}}^1, \dots, W_{\text{hh}}^p, \dots, W_{\text{hh}}^p, b_{\text{h}}^1, \dots, b_{\text{h}}^p, \dots, b_{\text{h}}^p, W_{\text{hy}}, b_{\text{y}})$ as:

$$\frac{\partial L^k}{\partial \phi} = \sum_{t=1}^T \frac{\partial L^k}{\partial h[t]} \frac{\partial h[t]}{\partial \phi} \quad (\text{C2})$$

$$= \sum_{t=1}^T \sum_{i=1}^t \frac{\partial L^k}{\partial h[t]} \cdot \left(\prod_{j=i+1}^t \frac{\partial h[j]}{\partial h[j-1]} \right) \cdot \frac{\partial h[i]}{\partial \phi} \quad (\text{C3})$$

This recursive computation captures the temporal dependency of the hidden states across multiple time steps.

C.2.1 More detailed explanation

Based on the update equation (6), each $h[t]$ is computed recursively from its previous state $h[t-1]$. In our implementation using PyTorch, the computational graph is automatically constructed during the forward pass. This graph stores: (1) intermediate values (like $h[t]$), (2) dependencies (how $h[t]$ is computed from $h[t-1]$, weights, and inputs). As a result, PyTorch can automatically compute partial derivatives such as $\frac{h[j]}{h[j-1]}$ using autograd.

Using the chain rule through time, the gradient of the loss with respect to each intermediate hidden state can be expressed as:

$$\frac{\partial L^k}{\partial h[t]} = \frac{\partial L^k}{\partial h[T]} \cdot \left(\prod_{j=t+1}^T \frac{\partial h[j]}{\partial h[j-1]} \right) \quad (\text{C4})$$

where $\frac{\partial L^k}{\partial h[T]}$ can be directly computed from the loss function in our experiments. So, it is possible to get $\frac{\partial L^k}{\partial h[t]}$. In addition, $\frac{\partial h[t]}{\partial \phi}$ can be computed by autograd. Thus, BPTT effectively propagates the gradients backward through time, allowing parameter updates via gradient-based optimization.

Nevertheless, ReLaX-net is also compatible with alternative training methods such as DFA-based [69] or adjoint-based methods [70].

C.3 Cross Entropy

Cross-entropy is a standard loss function used in classification tasks, which measures the dissimilarity between a true distribution \mathbf{p} and an estimated distribution \mathbf{q} . In most classification settings, the ground truth \mathbf{p} is represented as a one-hot encoded vector, and \mathbf{q} is the probability distribution output by the model (e.g., through a softmax layer). For discrete distributions \mathbf{p} and \mathbf{q} over $C \in \mathbb{N}$ classes, where p_c and q_c express the \mathbf{p} and \mathbf{q} probability on the class $c = 1, \dots, C$, the cross-entropy is computed as:

$$H(\mathbf{p}, \mathbf{q}) = - \sum_{c=1}^C p_c \log q_c \quad (\text{C5})$$

For the image classification task (SVHN), we set $C = 10$ (digits 0 through 9). (see subsection C.8 for SVHN dataset) For the next-token prediction task (Shakespeare corpus), we use $C = 43$, which corresponds to the number of unique tokens after pre-processing. (see subsection C.9 for Shakespeare corpus dataset) This loss encourages the model to assign high probability to the correct class while penalizing incorrect predictions.

C.4 Adaptive Moment Estimation (Adam)

Adam [68] is one of the most common optimization method in machine learning. It combines the benefits of two other popular methods: momentum [71] and RMSProp [72]. Given a parameter ψ_t , loss gradient $g_t = \nabla_{\psi} L_t$ at time step t , Adam uses two kinds of moments:

First moment (mean):

$$m_t = \beta_1 m_{t-1} + (1 - \beta_1) g_t \quad (\text{C6})$$

Second moment (uncentered variance):

$$v_t = \beta_2 v_{t-1} + (1 - \beta_2) g_t^2 \quad (\text{C7})$$

where β_1, β_2 are exponential decay rates for the moving averages. The first moment m_t smooths the gradient similarly to momentum, while the second moment v_t adapts the learning rate similarly to Root Mean Square Propagation (RMSProp).

To correct the bias introduced during initialization, Adam performs the following bias corrections:

$$\hat{m}_t = \frac{m_t}{1 - \beta_1^t} \quad (\text{C8})$$

$$\hat{v}_t = \frac{v_t}{1 - \beta_2^t} \quad (\text{C9})$$

Finally, the parameters are updated as:

$$\theta_{t+1} = \theta - \alpha_{\text{adam}} \cdot \frac{\hat{m}_t}{\sqrt{\hat{v}_t + \epsilon}} \quad (\text{C10})$$

In our experiments, we used $\alpha_{\text{adam}} = 0.001$, $\beta_1 = 0.9$, $\beta_2 = 0.999$, $\epsilon = 10^{-8}$, which are default values on Adam.

C.5 Initialization of the Hidden Layer Parameters

Deep neural networks are often susceptible to the problems of vanishing and exploding gradients, which can severely affect convergence during training. Appropriate initialization of weights plays a crucial role in maintaining the stability of the forward and backward signal propagation across layers.

In this study, we employ a widely used initialization strategy depending on the choice of activation function for a layer with λ_{in} inputs and λ_{out} outputs:

Kaiming Initialization (He Initialization) [60]:

$$w_{ij} \sim U\left(-\sqrt{\frac{6}{\lambda_{\text{in}}}}, \sqrt{\frac{6}{\lambda_{\text{in}}}}\right) \quad (\text{C11})$$

where w_{ij} expresses the values of weight matrices. This scaling preserves the variance of activations through ReLU layers, and is appropriate for models with ReLU as an activation function. In this study, this method is used because ReLU is selected as the activation function.

The strength of the residual connection, which is not a weight parameter, is an exception at the point of initialization. It is set to 1.0 at first, and it is changed during training.

C.6 Validation Dataset

To evaluate and tune our model, we created a validation dataset by splitting the original training dataset into two parts using a 9 : 1 ratio. The larger portion was used to train the model, while the smaller portion was reserved for validation purposes. This validation dataset is used in tuning hyperparameters, such as the number of hidden units in a layer or the number of weight switching steps in the ReLaX-Net structure. The resulting training dataset was also shuffled before use in mini-batch training, which is described in subsection C.7.

C.7 Mini-batch Gradient Descent

As we explained in subsection C.4, we train the model with BPTT, which is a kind of a gradient-based (gradient descent) method. At the same time, we use Mini-batch Gradient Descent, which is the middle ground between Gradient Descent and Stochastic Gradient Descent (SGD). Gradient Descent computes the exact gradient of the loss over the entire training set, then takes one parameter update. While precise, this approach can be computationally intensive, especially for large datasets. SGD instead

approximates that gradient by computing it on a single random example and immediately updating the model. Although this results in faster updates, it introduces significant variance and noise into the optimization process. Mini-Batch Gradient Descent serves as a compromise between these two methods. In our study, we use mini-batches of size N_{batch} for both training and evaluation on the SVHN classification task. Each update step is based on the gradient computed over one mini-batch. This method offers the computational efficiency of SGD while reducing the variance in gradient estimates, which contributes to more stable and effective learning. Additionally, mini-batch processing is well-suited to modern parallel hardware architectures, making it the default choice for training deep models.

C.8 SVHN Classification

In this subsection, we describe the experimental setup used to evaluate ReLaX-Net on an image classification task. The objective of this experiment is to demonstrate how ReLaX-Net can improve the performance of a recurrent neural network compared to a conventional RNN.

We train the model using the Street View House Numbers (SVHN) dataset [59], which contains over 600000 color images of digits (0–9) extracted from real-world Google Street View photographs. Specifically, the dataset includes 73257 images for training and 26032 images for testing. Each image is a cropped digit, making this a ten-class classification problem.

Among image classification tasks, MNIST (Modified National Institute of Standards and Technology) [73] may be the most popular dataset because of its simplicity. Compared to MNIST, the SVHN dataset poses a more challenging classification task due to its real-world complexity, color variations, and background clutter. We selected SVHN over MNIST to better assess the expressivity and performance improvements provided by the ReLaX-Net architecture under more practical conditions.

To avoid over-fitting, we used data augmentation techniques on the SVHN dataset. These techniques are explained in subsection C.8.1, C.8.2, C.8.3 and C.8.4. Then, we explain how we train ReLaX-Net with SVHN in C.8.5

C.8.1 Randomcrop and padding

Each image in the SVHN dataset is a $32 \times 32 \times 3$ RGB image stored as unsigned 8-bit integers. To introduce spatial variation and improve generalization, we first pad each image by 4 pixels on all sides, expanding its dimensions to 40×40 . After padding with pure black that all components are 0, we extract a randomly located 32×32 crop from the padded image. This augmentation simulates minor translations as well as zoom-in and zoom-out effects, encouraging the model to learn spatial invariance in its representations.

C.8.2 Color jitter

Following spatial augmentation (random crop and padding), we apply random color jittering to simulate changes in lighting and scene conditions. Specifically, we perturb the brightness, contrast, and saturation of each image by up to $\pm 10\%$, and adjust the

hue by up to $\pm 5\%$. These transformations help the model become robust to variations commonly observed in real-world street imagery. Given that the SVHN dataset is derived from natural photographic scenes, such augmentations serve to better align the training distribution with the expected variability.

C.8.3 Add gaussian noise

We convert SVHN values from $[0, 255]$ integer to $[0, 1]$ float values by dividing them by 255 with converting it to a tensor. To further improve generalization, we inject pixel-wise Gaussian noise (standard deviation of the noise is 0.005). This augmentation encourages the model to become invariant to minor artifacts such as compression noise or small, irrelevant details and helps to reduce the risk of overfitting.

C.8.4 Normalize

After applying noise, we normalize each RGB channel per images to have zero mean and unit variance, assuming the inputs are already scaled to the $[0, 1]$ range. This normalization procedure accelerates convergence by ensuring consistent gradient flow across different input dimensions. Finally, each image, originally a $32 \times 32 \times 3$ tensor, is reshaped into a 3072-dimensional vector. These vectors are then used as inputs to the ReLaX-Net, repeatedly.

C.8.5 SVHN training

Then, we train the models with BPTT stated in subsection C.2. As we explained in subsection C.2, the input is expressed as a vector $x^k[t] \in \mathbb{R}^X$ where k is the image (data) index in the mini-batch data, whose size is N_{batch} . In this image classification task, we input the same image x_{image} repeatedly. (In other words, $x^k[t] = x_{\text{image}} = \text{const}$ for $t = 0, \dots, L_T - 1$.)

As we use the output \hat{y}^k from the equation 4 as the prediction result in the numerical experiments

$$L_k = l(y_{\text{target}}^k, \hat{y}^k) \tag{C12}$$

Then, we trained the model with Adam.

C.9 Next Token Prediction

One of the main reasons RNNs are widely studied is their natural ability to process sequential data [54]. In this section, we evaluate the ReLaX-Net on a time-series prediction task, specifically next-token prediction. Although a deep feedforward network may work with sequential data by simultaneously inputting all tokens as part of a large input vector, ReLaX-Net is structurally distinct due to its recurrent dynamics and weight-switching mechanism. We therefore employ a different input strategy that befits ReLaX-Net, which differs from just repeating the DNN as explained in section C.10. This difference makes it particularly interesting to study how ReLaX-Net behaves in sequential tasks compared to conventional models.

Next-token prediction involves learning a model that, given a sequence of past inputs, predicts the most likely next symbol or token in the sequence. This task captures the temporal dependencies in the data and is commonly used in language modeling and other autoregressive applications.

C.9.1 Shakespeare dataset

For the next-token prediction task, we use a dataset derived from the Folger Shakespeare Library’s digital editions [62]. The dataset consists of plain-text versions of Shakespeare’s plays, containing a total of 9044939 characters. To convert the text into a trainable format suitable for RNN input, we applied a series of preprocessing and tokenization steps, described in subsection C.9.2.

C.9.2 Tokenization

Before tokenization, the text is first preprocessed to simplify further processing. All uppercase letters are converted to lowercase, and variant characters are mapped to their modern equivalents in the English alphabet. Infrequent characters, defined as those with an occurrence rate below 0.01%, are replaced with a special placeholder symbol to limit the vocabulary size.

Next, we construct a vocabulary by counting the frequency of all fixed-length substrings (n-grams) within the full corpus. In this experiment, we set $n = 1$, so the tokens correspond to individual characters. Then, we can build vocabulary by giving an index to the tokens. The placeholder character is assigned index 0 in the vocabulary. All other characters are assigned indices based on frequency, with the more frequent characters given lower index values.

The final vocabulary contains all characters that exceed the minimum frequency threshold. Using this vocabulary, we tokenize the Shakespeare text. For each position in the text, we identify the character that exists in the vocabulary. If a match is found, the corresponding token is emitted, and the pointer is advanced. If no valid match is found, the placeholder token is emitted, and the pointer advances by one character. Finally, we slice the integer array into a contiguous 90% train / 10% validation split.

That integer array is reshaped into fixed-length windows of size $T + 1$. The length of each sample is $T + 1$. Inputs are the first T tokens, and targets are the last $T + 1$ -th token. These (input, target) pairs are what the ReLaX-Net actually consumes during training.

C.9.3 Time series input

The input can be expressed as a sequence $\mathbf{x}^k = (x^k[1], \dots, x^k[T])$, $x^k[t] \in \mathbb{R}^X$ where k is the data index in the mini-batch data. In this next token prediction task, we embed the token scalars $x[t]$ to embedding vectors $x_e[t] \in \mathbb{R}^{36}$ before inputting them into RNN as an input $\mathbf{x}_e^k = (x_e^k[1], \dots, x_e^k[T])$.

As in the image classification task, we obtain the output \hat{y}^k from the equation 4 as the prediction result in the numerical experiments

$$L_k = l(y_{\text{target}}^k, \hat{y}^k) \tag{C13}$$

Then, we trained the model with Adam.

C.9.4 Variational RNN

Unlike image-based tasks, textual data does not lend itself to spatial augmentations. To mitigate overfitting in the next-token prediction task, we apply a regularization technique known as variational dropout [61], which is specifically adapted for RNNs.

Unlike standard dropout, where dropout masks are independently resampled at every time step, variational dropout applies fixed dropout masks across both the temporal and depth (layer) dimensions. This preserves temporal consistency and prevents information leakage that may arise from fluctuating dropout patterns during sequence modeling.

To implement variational dropout, on each mini-batch dataset, we generate three kinds of dropout masks per mini-batch: one each for the input-to-hidden $M_{\text{xh}}^{\text{dp}}$, hidden-to-hidden $M_{\text{hh}}^{\text{dp}}$, and hidden-to-output $M_{\text{hy}}^{\text{dp}}$ connections. These masks are sampled from a Bernoulli distribution and applied as multiplicative noise before the corresponding matrix operations as follows:

$$x^{\text{dp}}[t] := M_{\text{xh}}^{\text{dp}}x[t] \quad (\text{C14})$$

$$h^{\text{dp}}[t] := M_{\text{hh}}^{\text{dp}}h[t] \quad (\text{C15})$$

$$\hat{y}^{\text{dp}} := W_{\text{hy}}(M_{\text{hy}}^{\text{dp}}h[L_{\text{T}}] + b_{\text{y}}) \quad (\text{C16})$$

Using them instead of $x[t], h[t], \hat{y}$, the update equation (3) can be rewritten:

$$h^{\text{dp}}[t] = M_{\text{hh}}^{\text{dp}}(\alpha h^{\text{dp}}[t-1] + f(W_{\text{xh}}x^{\text{dp}}[t] + W_{\text{hh}}[t]h^{\text{dp}}[t-1] + b_{\text{h}}[t])) \quad (\text{C17})$$

The consistent masking across time steps ensures stable dynamics while promoting generalization.

Although this dropout method in variational RNN makes it possible to prevent overfitting, it also results in performance increase saturations at the same time.

C.9.5 NLP performance decrease with large number of distinct weights L_{W}

In Fig. 6, ReLaX-Net shows a different trend on results on a NLP task compared to image classification. Especially, the error rate increases when the number of distinct weights L_{W} is large. This is the opposite of the expected effect, as more parameters generally imply better performance for neural networks. To further investigate the details of next token prediction tasks, we show the change of loss changing during the training epochs.

Supplementary Figure C1 shows the change of test loss on the different L_{W} . We prepare 5 trials, and the pastel colors show the standard deviations. The epoch 200 values are the results that Fig. 6 show. As can be seen, the test loss flattens at a higher value when L_{W} increases (compare pink and red lines in Supplementary Figure C1). The flat shape indicates that ReLaX-Net cannot increase its performance with large

epochs. Generally speaking for such characteristics, there are some possible causes: insufficient dataset, inappropriate parameters (learning rate, initialization), dropout effect and gradient vanishing/exploding etc. Considering that the performance on the $L_W = 6$ case is better than the ones on larger L_W cases, there should be enough data, appropriate parameters, and a dropout setting. Thus, gradient vanishing/exploding is considered to be the cause of the performance decrease. In particular, with L_W sufficiently smaller than the number of temporal steps (here: $L_T = 12$), every layer is repeated closer to the output section, allowing it to be trained even if gradients vanish.

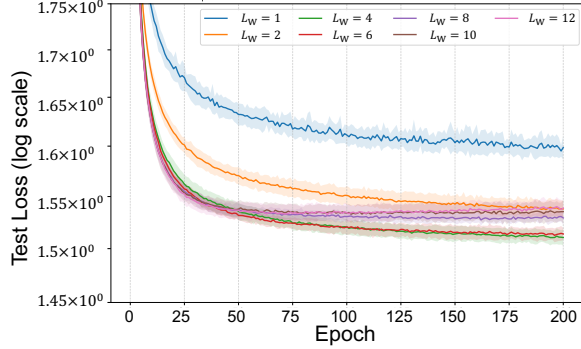


Fig. C1 — Epochs vs ReLaX-Net Performance on NLP. Test Loss changes as epoch increases. The loss values generally decrease as training progresses. The loss learning curves flatten out at higher values as L_W increases, which is likely caused by the effect of gradient vanishing/exploding.

C.10 Repeating DNNs and ReLaX-net

ReLaX-Net shares structural similarities with models that are constructed by repeating deep neural networks. In principle, a repeated DNN-structure with a few layers will yield a similar sequence of operations as ReLaX-Net. If the number of distinct weights L_W divides the number of time steps (layers) L_T , ReLaX-net corresponds to a stateless RNN where the fundamental unit are L_W weights, repeated several times.

However, ReLaX-net is constructed to also handle cases where layers are only partially repeated. Similarly, we allow the input to be injected at different time steps. This allows ReLaX-Net to handle sequential inputs over time, rather than requiring all input data to be presented simultaneously. This makes ReLaX-Net suitable for time-series tasks, where inputs arrive incrementally such as the NLP task shown in the main manuscript.

Note, that in the field of photonic computing, repeating simple layers has been proposed and physically demonstrated in the field of based on Diffractive Deep Neural Networks (D²NN) [13, 74]. Note, that for ReLaX-net we would consider the sets of diffractive layers of a D²NN as a single hidden layer, as the nonlinear function is only applied once at the read-out. In that sense, D²NN can be considered to have demonstrated the case of a stateless RNN with $1 = L_W < L_T$. These platforms are

promising candidates for implementing a full ReLaX-net like structure with several distinct layers.

In general, in ReLaX-Net, only the network weights need to be switched or cycled during operation, so that implementations of the activation function can be reused as much as possible (which also increases the uniformity of the nonlinear activation function across layers).

Consequently, ReLaX-Net can be viewed as an extended and more physically feasible variant of repeated DNN architectures. In this paper, we focussed on the simplest versions of a ReLaX-Net structure, with a periodic repetition structure. In principle, there is no need to choose this particular order, and aperiodic structures could also be used - which would not be possible by merely repeating a small multi-layer DNN several times.

Appendix D MNIST Classification

As explained in the main text, we used SVHN as a dataset instead of MNIST, which is arguably the most common benchmark for image classification in PNNs. MNIST is quite a simple task, where a lot of the classification accuracy can already be achieved by a linear system. We therefore found it insufficient for consistently showing trends and performance differences, as many models saturate performances. For reference, however, we show the results with MNIST in this section.

Supplementary Figure D2 shows the result of the MNIST image classification. Similar to the Fig. 5 results, ReLaX-Net outperforms standard RNNs with additional layers. However, the value improvement in both error rate and test loss is small. Furthermore, the error bars of the loss in Supplementary Fig. D2b are too large to distinguish the updates. Since the standard RNN has already achieved a quite low error and loss value, we consider that MNIST is too easy to highlight the performance differences in our settings. Furthermore, reducing the error rate from $\leq 5\%$ to $\leq 1\%$ is often only a question of finetuning data augmentation methods.

Appendix E Examples of SVHN Image Classification Performance

In the main text, we present ReLaX-Net’s performance on the image classification task using SVHN [59]. For reference, we supply some standard performance on this task in this section.

In Supplementary Table E3, we present performance examples for the SVHN image classification task. In the case of Fit-DNN [47] ($N = 100$, $L = 2$, which are parameters defined in [47]), the number of trainable parameters and the achieved accuracy of Folded-in-time Deep Neural Network (Fit-DNN) are comparable to those of the Standard RNN and ReLaX-Net. In the original study proposing SVHN [59], Linear Support Vector Machine (SVM) with Histogram of Oriented Gradients (HOG), which generates characteristic features, also demonstrated a similar performance. These results indicate that ReLaX-Net achieves a reasonable performance level compared with both a

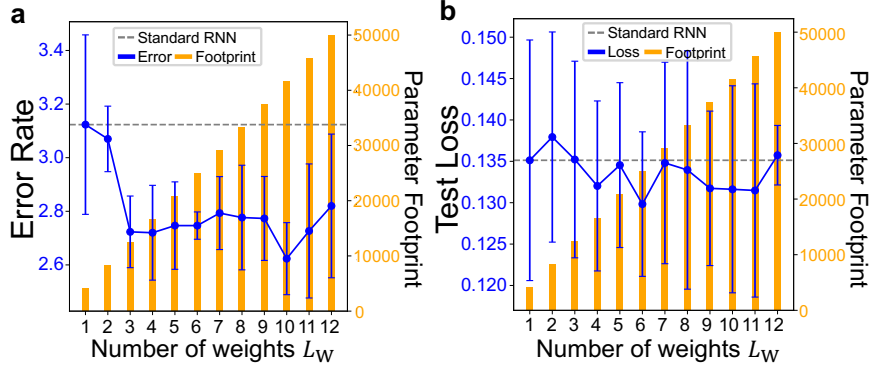


Fig. D2 —**ReLaX-Net Performance on Image Classification Tasks with MNIST.** The number of weights L_W is changed while keeping the number of layers L_T constant. **a, b** Error Rate and Parameter Footprint when varying L_W . Rate (a) and loss (b), and orange bars show the number of trainable parameters, corresponding to the hardware footprint. The gray dashed line is the performance of the stateless RNN limit for $L_W = 1$. While ReLaX-Net can outperform standard RNNs with additional layers like Fig. 5, the performance increase is small. Especially, the error bar of **b** is too large to distinguish the updates.

PNN (Fit-DNN [47]) and a conventional reference model used in the SVHN benchmark (Linear SVM with HOG [59]).

Table E3 —**SVHN Classification Performance Comparison.** ReLaX-Net achieves reasonable performance among other previous approaches. Models have different architecture separated into different components. “Input (Hidden, Output)” expresses the number of parameters in the input weight (hidden layers, output weight) as a multilayer perceptron. “Other” expresses the number of parameters coming from other components, such as the strength of residual connections. In addition, there are blanks in Human because we do not know how many parameters are used in the Human brain for image classification.

Model	SVHN Accuracy	Input	Hidden	Output	Other
Fit-DNN ($N = 100, L = 2$) [47]	78.9%	102,500	10,100	1,010	-
Standard RNN	79.5%	196,672	4,160	650	1
ReLaX-Net ($L_W = 12$)	82.6%	196,672	49,920	650	1
Linear SVM with HOG [59]	85.0%	-	-	-	1765
Human [59]	98.0%				

Appendix F Examples of Next Token Prediction

We worked on the next token prediction task with ReLaX-Net. A trained ReLaX-Net can be used as a generative model with input prompts. To illustrate its performance of the trained model intuitively, we show the examples of the NLP output at different training stages.

Supplementary Table F4 shows 20-character (here, a space is seen as one character) output sequences generated with the input prompt “to be, or not to be,” at different training epochs under the same setting as Fig. 6. The trained ReLaX-Net model generates successive characters following the given input. As training progresses, the outputs evolve from incomprehensible strings to increasingly reasonable sequences. This trend is the same among different L_W cases.

Table F4 —Output Examples on NLP Tasks. ReLaX-Net outputs when using ReLaX-Net as a generative model with the input prompt “to be, or not to be,” from the Fig. 6 setting. As training progresses, more coherent continuations appear. Note, that our models are far smaller than even GPT-2 and thus cannot be expected to produce full sentences consistently.

epoch	$L_W = 1$	$L_W = 4$	$L_W = 8$	$L_W = 12$
1	aiuer rol ruitam r-	me sous the the the	tttttttttttttttttt	are
100	and thoopple they so	and the state the st	akiccxeanxtny top th	and the state the st
200	and thee the king pe	and the stranger the	akicletn tay tprofray	my lord, and the cou

Appendix G ReLaX-Net with an Oscillator Network

As explained in Section 1, spintronics is a promising approach to achieve energy-efficient PNNs. In the PNN implementation with spintronics, nodes in hidden layers are something that oscillate, such as magnetic spins. Oscillator networks introduce nonlinearity into computing in a different way from the standard activation functions like ReLU. To investigate the generality regardless of the activation function, we conduct an experiment on ReLaX-Net where the nonlinear activations are achieved with oscillations.

Let the hidden states $h[t]$ evolve with the help auxiliary intermediate states $h_c^{(\kappa)} \in \mathbb{R}^H, \kappa \in [0, \dots, \eta]$ evolve according to:

$$h_c^{(0)} := h[t - 1] \quad (\text{G18})$$

$$h_c^{(\kappa+1)} = h_c^{(\kappa)} + \Delta t \cdot \left(\left(\gamma_p - \gamma_{nl} \left(h_c^{(\kappa)} \right)^2 \right) h_c^{(\kappa)} + W_{xh} x[t] + b_h[t] \right) \quad (\text{G19})$$

$$h[t] = \alpha h[t - 1] + h_c^{(\eta)}, \quad (\text{G20})$$

where $\gamma_p, \gamma_{nl} \in \mathbb{R}$ are the parameters of the spintronics system trainable and $\Delta t \in \mathbb{R}_{>0}$ is the parameter for the integration over time in the numerical calculation. In our experiment, Δt is fixed such that η is 3. This equation corresponds to the simplified Slavin’s model [18] as follows:

$$\frac{dx}{dt} = -\gamma x + I(t)x(1 - x) \quad (\text{G21})$$

where γ is the damping parameter, x is the nodes state and $I(t)$ is the time-dependent drive.

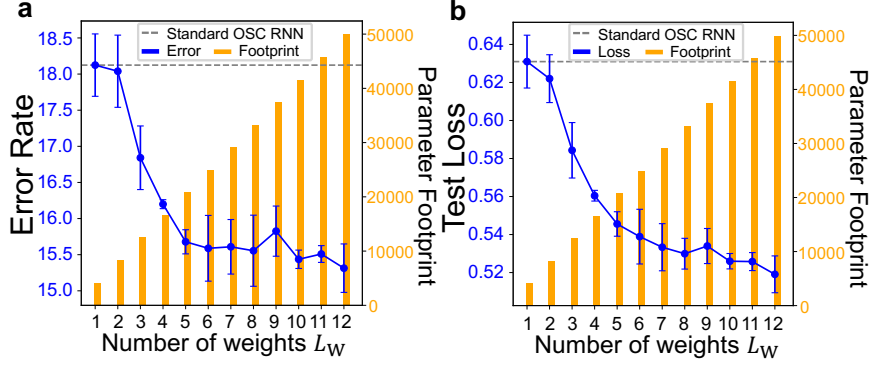


Fig. G3 —**ReLaX-Net Performance with Oscillator Network Performance.** **a:** Error Rate **b:** Test Loss (Crossentropy) Like ReLaX-Net with ReLU, the error and loss (blue plot) decrease as the number of parameters (orange bars) increase. This means that ReLaX-Net with Oscillator Network has the same advantages that ReLaX-Net with ReLU has.

Supplementary Figure G3 shows the results of the numerical experiment of ReLaX-Net with this Oscillator Network on SVHN classification tasks. The number of training epochs was 900. Generally speaking, we observe the same trends as the results for a more traditional ReLU network shown in the main manuscript Fig. 5. This shows that ReLaX-Net is not limited to a particular activation function.

Appendix H Ideal Parameters and Repetition Effect

One of the key differences of ReLaX-Net from Deep Neural Network is the repetitive usage of the network. Repetition can create deep layered structures, which are known for enhancing performance. On the other hand, it is also known that RNNs fail at learning sequence that are too long [64], corresponding to the case of many repetitions. To further investigate the repetition effect in detail, we changed the time step L_T and the number of weights L_W when keeping the number of nodes per hidden layer H . This is different from the case shown in the main manuscript, where H was modified to keep the total number of trainable parameters fixed.

Supplementary Figure H4 shows a 2D plot of these more detailed numerical investigations. Here, higher L_W have proportionally more trainable parameters. Accordingly, the cases having more parameters, when L_W is larger, achieve better results (see the lower test error and loss in Supplementary Fig. H4). In addition, we see that for most cases the results with $L_W < L_T$ are better than the results with $L_W = L_T$. This shows that repetition is beneficial in most cases and enhances the model’s performance. However, the optimal number of repetitions does not follow a clear rule. For a particular network on a particular task, it is likely necessary to optimize the number of repetitions and other hyperparameters.

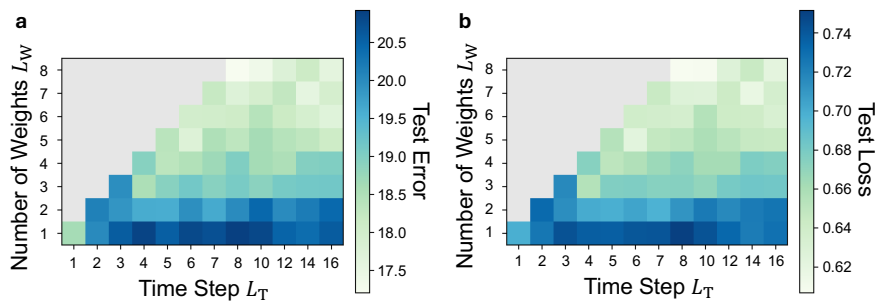


Fig. H4 —ReLaX-Net Performance Heatmap on SVHN Classification When the Number of Parameters in One Layer H is Fixed. **a:** Error. **b:** Loss. Generally speaking, large L_W results in better performance. The best performance for a fixed parameter budget (fixed L_W) is, in general, not the case when $L_W = L_T$. This means that repetitive usage can enhance the performance. By definition, $L_W > L_T$ is not a valid setting, and gray cells indicate such impossible configurations.